

## RESEARCH ARTICLE



# Hydroxymethylglutaryl-CoA reductase activity is essential for mitochondrial $\beta$ -oxidation of fatty acids to prevent lethal accumulation of long-chain acylcarnitines in the mouse liver

Edgars Liepinsh<sup>1,2</sup> | Liga Zvejniece<sup>1</sup> | Laura Clemensson<sup>3</sup> | Melita Ozola<sup>1,2</sup> |  
 Edijs Vavers<sup>1</sup> | Helena Cirule<sup>1</sup> | Stanislava Korzh<sup>1</sup> | Sandra Skuja<sup>2</sup> |  
 Valerija Groma<sup>2</sup> | Monta Briviba<sup>4</sup> | Solveiga Grinberga<sup>1</sup> | Wen Liu<sup>3</sup> |  
 Paweł Olszewski<sup>3</sup> | Mélissa Gentreau<sup>3</sup> | Robert Fredriksson<sup>3</sup> |  
 Maija Dambrova<sup>1,2</sup> | Helgi B. Schiöth<sup>3</sup>

<sup>1</sup>Latvian Institute of Organic Synthesis, Riga, Latvia

<sup>2</sup>Riga Stradins University, Riga, Latvia

<sup>3</sup>Uppsala University, Uppsala, Sweden

<sup>4</sup>Latvian Biomedical Research and Study Centre, Riga, Latvia

## Correspondence

Edgars Liepinsh, Latvian Institute of Organic Synthesis, Riga, Latvia.

Email: [ledgars@farm.osi.lv](mailto:ledgars@farm.osi.lv)

Helgi B. Schiöth, Uppsala University, Uppsala, Sweden.

Email: [helgi.schioth@neuro.uu.se](mailto:helgi.schioth@neuro.uu.se)

## Funding information

Vetenskapsrådet, Grant/Award Numbers: 2019-01066, 2022-00562; Novo Nordisk Fonden; Latvijas Zinātnes Padome, Grant/Award Number: LZP-2023/1-0287; Horizon 2020 Framework Programme, Grant/Award Numbers: 857394, 857287

## Abstract

**Background and Purpose:** Statins are competitive inhibitors of 3-hydroxy-3-methylglutaryl coenzyme A (HMG-CoA) reductase (HMGCR), and exert adverse effects on mitochondrial function, although the mechanisms underlying these effects remain unclear. We used a tamoxifen-induced *Hmgcr*-knockout (KO) mouse model, a multi-omics approach and mitochondrial function assessments to investigate whether decreased HMGCR activity impacts key liver energy metabolism pathways.

**Experimental Approach:** We established a new mouse strain using the Cre/loxP system, which enabled whole-body deletion of *Hmgcr* expression. These mice were crossed with Rosa26<sup>Cre</sup> mice and treated with tamoxifen to delete *Hmgcr* in all cells. We performed transcriptomic and metabolomic analyses and thus evaluated time-dependent changes in metabolic functions to identify the pathways leading to cell death in *Hmgcr*-KO mice.

**Key Results:** Lack of *Hmgcr* expression resulted in lethality, due to acute liver damage caused by rapid disruption of mitochondrial fatty acid  $\beta$ -oxidation and very high accumulation of long-chain (LC) acylcarnitines in both male and female mice. Gene expression and KO-related phenotype changes were not observed in other tissues. The progression to liver failure was driven by diminished peroxisome formation, which resulted in impaired mitochondrial and peroxisomal fatty acid metabolism, enhanced glucose utilization and whole-body hypoglycaemia.

**Conclusion and Implications:** Our findings suggest that HMGCR is crucial for maintaining energy metabolism balance, and its activity is necessary for functional

**Abbreviations:** ALT, alanine transaminase; ChREBP, carbohydrate-responsive element-binding protein; CPT1, carnitine palmitoyltransferase-1; FAO, fatty acid oxidation; FDR, false discovery rate; HMGCR, 3-hydroxy-3-methylglutaryl CoA reductase; NEFA, non-esterified fatty acid; PCA, principal component analysis.

This is an open access article under the terms of the [Creative Commons Attribution-NonCommercial-NoDerivs](https://creativecommons.org/licenses/by-nc-nd/4.0/) License, which permits use and distribution in any medium, provided the original work is properly cited, the use is non-commercial and no modifications or adaptations are made.

© 2024 The Authors. *British Journal of Pharmacology* published by John Wiley & Sons Ltd on behalf of British Pharmacological Society.

mitochondrial  $\beta$ -oxidation. Moreover, statin-induced adverse reactions might be rescued by the prevention of LC acylcarnitine accumulation.

#### KEYWORDS

HMG-CoA reductase, mitochondria, Rosa26<sup>Cre</sup> mice, statins, tamoxifen-induced knockout mouse model

## 1 | INTRODUCTION

The enzyme 3-hydroxy-3-methylglutaryl coenzyme A (HMG-CoA) reductase (HMGR) catalyses the rate-limiting step of sterol and isoprenoid biosynthesis (Alexander et al., 2021, 2017). HMGR catalyses HMG-CoA conversion to mevalonate and can be competitively inhibited by statins, which are widely prescribed to prevent the progression of atherosclerosis and coronary heart disease because they reduce blood cholesterol levels (Goldstein & Brown, 2015; Newman et al., 2019). To treat high cholesterol levels, approximately 25% of the older adult population worldwide has been prescribed statins. However, statin treatment induces several adverse effects, including hepatotoxicity and myopathy, which are the more common reasons for treatment termination (Mollazadeh et al., 2021; Newman et al., 2019; Penson et al., 2022). Despite the adverse effects, statins are broadly and increasingly prescribed, and a high number of patients taking statins are at risk of side effects (Colantonio et al., 2019; Virani et al., 2017). The molecular mechanisms, particularly the biochemistry, underlying the different side effects induced by statins remain poorly understood. To date, studies have shown that statin-induced myopathy is associated with the inhibition of mitochondrial electron transfer chain complexes (Schirris et al., 2015). Changes in fatty acid oxidation (FAO) in mitochondria and peroxisomes have not yet been assessed in animal models with *Hmgcr* knocked out.

The heart, skeletal muscles and liver largely depend on fatty acid metabolism in mitochondria and peroxisomes. Dysfunctional mitochondrial FAO is related to several diseases, such as inherited fatty acid oxidation disorders (FAODs) (Knottnerus et al., 2018; Merritt et al., 2018), heart failure and myocardial infarction (Dambrova et al., 2022), and to certain drug treatments, such as nonsteroidal anti-inflammatory drugs that cause liver injury (Begrache et al., 2011; Di Pasqua et al., 2022; Pessayre et al., 2012), by inducing the accumulation of long-chain (LC) fatty acids and their metabolic intermediates.

LC acylcarnitines are fatty acid metabolites that are synthesized from carnitine and LC acyl-CoA by the mitochondrial enzyme carnitine palmitoyltransferase-1 (CPT1), which support the transport of LC fatty acids to mitochondria where they are oxidized (Dambrova et al., 2022; Shriver & Manchester, 2011). Decreased mitochondrial fatty acid metabolism in different pathological states, such as during starvation in patients with FAOD or with myocardial ischaemia, increases the levels of LC acylcarnitines (Ahmad et al., 2016; Liepinsh et al., 2016; McCoin et al., 2015; Wanders

### What is already known

- Statins inhibit HMGR and exert adverse effects.
- Deletion of HMGR in mice resulted in the acquisition of a profoundly negative phenotype.

### What does this study add

- Deletion of HMGR induces mitochondrial dysfunction and accumulation of long-chain acylcarnitines.
- HMGR activity is crucial for functional fatty acid  $\beta$ -oxidation.

### What is the clinical significance

- Statin-induced adverse reactions might be rescued by the prevention of long-chain acylcarnitine accumulation.

et al., 2020). High levels of LC acylcarnitines induce cell death because they inhibit oxidative phosphorylation and induce reactive oxygen species (ROS) production (Liepinsh et al., 2016; Primassin et al., 2008; Tominaga et al., 2008). In inherited FAODs characterized by very high levels of LC acylcarnitines, patients exhibit cardiac, skeletal muscle and liver damage that can lead to sudden death (Begrache et al., 2011; Di Pasqua et al., 2022; Pessayre et al., 2012; Wanders et al., 2020).

Tissue-specific *Hmgcr*-knockout (KO) mouse models have been previously developed, and studies based on these models have revealed the acquisition of a profoundly negative phenotype after *Hmgcr* gene KO in the liver, muscle, adipose tissue,  $\beta$  cells or T cells (De Giorgi et al., 2020; Lacher et al., 2017; Osaki et al., 2015; Takei et al., 2020; Yeh et al., 2018). In previous studies, the critical role played by the mevalonate pathway in cell survival was identified (Lacher et al., 2017; Nagashima et al., 2012). Liver-specific dolichol depletion was found to be at least partially responsible for endoplasmic reticulum (ER) stress. However, because the ER is structurally connected to all metabolically active organelles, including mitochondria and peroxisomes (Di Cara et al., 2023), and actively

participates in lipid metabolism, ER stress might be induced by a strong metabolite-related stimulus, such as lipid overload. Lacher et al. (2017) demonstrated that *Hmgcr*-KO resulted in protein deficiency in the prenylation pathway and that *Hmgcr* was indispensable for the survival of T cells. Moreover, tissue-specific KO of *Hmgcr* in  $\beta$  cells, liver cells or adipose tissue cells led to organ failure and affected the turnover of energy substrates and energy homeostasis throughout the whole body (De Giorgi et al., 2020; Lacher et al., 2017; Osaki et al., 2015; Takei et al., 2020; Yeh et al., 2018). However, to date, the intracellular changes in the energy metabolism pathways of *Hmgcr*-KO animals have not been characterized.

To elucidate the pathways related to the detrimental effects observed in *Hmgcr*-KO mice and, in particular, to understand the mechanism underlying the negative phenotype acquired by patients taking statins, we established a new mouse strain using the Cre/loxP system, which enabled whole-body deletion of *Hmgcr* expression. These mice were crossed with *Rosa26<sup>Cre</sup>* mice and treated with tamoxifen to delete *Hmgcr* in all cells. We performed transcriptomic and metabolomic analyses, and thus evaluated time-dependent changes in metabolic functions, to identify the pathways leading to cell death in *Hmgcr*-KO mice. We demonstrate that *Hmgcr*-KO mice develop early-onset lethal liver failure associated with dysfunction of mitochondrial FAO of LC fatty acids in the liver, which leads to the accumulation of LC acylcarnitines and disturbed cellular metabolism.

## 2 | METHODS

### 2.1 | Generation of *Hmgcr* floxed mouse line

The *Hmgcr* floxed mouse line (C57BL/6N-*Hmgcr<sup>em1Lclem/Lclem</sup>*) was created by CRISPR/Cas9-mediated genome engineering (Cyagen Biosciences Inc., Guangzhou, China). The gRNA to mouse *Hmgcr* gene, the donor vector containing loxP sites, and Cas9 mRNA were co-injected into fertilized mouse eggs to generate targeted conditional KO offspring. F0 founder animals were identified by polymerase chain reaction (PCR) followed by sequence analysis, which were bred to wild-type mice to test germline transmission and F1 animal generation.

### 2.2 | Generation of *Hmgcr*-KO mice

LoxP sites around exon 5 of the *Hmgcr* gene enable the Cre-mediated excision for a functional *Hmgcr*-KO. Homozygous mice are used for maintenance and for cross-breeding with Cre-expressing *Rosa26<sup>Cre</sup>* (B6.129-Gt(*Rosa*)26Sor<sup>tm1(cre/ERT2)Tyj/J</sup>) mice (The Jackson Laboratory). The mice have no phenotype unless cross-bred with Cre-expressing mice and are treated with tamoxifen. Homozygous *Rosa26<sup>Cre</sup>* mice were used for cross-breeding with floxed *Hmgcr* mice.

### 2.3 | Genotyping

Mice were approximately 14 days old when tail biopsies were taken for genotyping. Genomic DNA was extracted from tail biopsies, and PCR analysis was conducted to amplify a 217-bp (homozygote), 157-bp (wild-type) and 217/157-bp (heterozygote) region using HOT FIREPol® Blend Master Mix Ready to Load with 12.5-mM MgCl<sub>2</sub>, 5× (Solis BioDyne, Tartu, Estonia), and with the following primer sets: forward GGTGTTTCAGTGCGTGTTCATTAC and reverse AAGCCT-CATGAAACCCAGATTGAC. The following thermocycler programme was used: 95°C for 15 min; then 95°C for 20 s; 58°C for 45 s; 72°C for 1 min for 33 cycles; then 72°C for 10 min and hold at 4°C. The PCR product was separated on 2% agarose gels run at 90 V for 60 min.

Next, homozygous *Hmgcr* floxed mice were bred with homozygous *Rosa26<sup>Cre</sup>* mice, resulting in a new double-mutant mouse line called B6.Cg-Gt(*Rosa*)26Sor<sup>tm1(cre/ERT2)Tyj</sup> >*Hmgcr*<sup>em1Lclem</sup>/Lclem (*Hmgcr*-KO). Those double-mutant heterozygote mice were used for future breeding until we found double-mutant homozygote males and females, which were used to maintain the mouse line. *Hmgcr*<LoxP> locus genotyping was performed as described above. B6.129-Gt(*Rosa*)26S or tm1(cre/ERT2)Tyj/J locus was genotyped using the same PCR parameters, but the primer set for genotyping the wild-type allele was forward CTGGCTTCTGAGGACCG and reverse CCGAAAATCTGTGGGAAGTC (product size of 198 bp) and mutant allele forward CGTGATCTGCAACTCCAGTC and reverse AGGCAAATTTGGTGTACGG (product size of 150 bp).

### 2.4 | Experimental animals

Animal studies are reported in compliance with the ARRIVE guidelines (Percie du Sert et al., 2020) and with the recommendations made by the *British Journal of Pharmacology* (Lilley et al., 2020). Experimental procedures were performed in accordance with the guidelines reported in the EU Directive 2010/63/EU and local laws and policies. All procedures were approved by the Latvian Animal Protection Ethical Committee of the Food and Veterinary Service in Riga, Latvia. A total of 25 adult (with added 10 females for 5 day experiment) 12-week-old male and female mice were used in the experiment: 12 floxed (7 females and 5 males; *Hmgcr<sup>LoxP/LoxP</sup>*-*Rosa26<sup>WT/WT</sup>*) and 13 *Hmgcr* conditional KO (8 females and 5 males; *Hmgcr<sup>LoxP/LoxP</sup>*-*Rosa26<sup>Cre/WT</sup>*). All animals were housed under standard conditions (21–23°C, 12-h dark–light cycle), with unlimited access to standard food (R70 Lactamin AB, Mjölby, Sweden) and water in an individually ventilated cage housing system (cage size 38 × 19 × 13 cm, Allentown, Inc., Allentown, NJ, USA). Each cage contained bedding consisting of EcoPure™ Shaving's wood chips (Datesand, Cheshire, UK), nesting material and a wooden block from TAPVEI (Paekna, Estonia). For enrichment, transparent tinted (red) nontoxic durable polycarbonate Safe Harbor Mouse Retreat (Animalab, Poznań, Poland) was used. Mice were housed with three to five animals per standard cage. The floxed and KO mice were housed separately.

## 2.5 | Tamoxifen treatment

To induce the *Hmgcr* gene KO, we used tamoxifen in the chow (A155T70212, ssniff Spezialdiäten GmbH) at a dose of 210 mg·kg<sup>-1</sup> of tamoxifen citrate-containing chow that, according to food intake data, is equal to a dose of 14 mg·kg<sup>-1</sup>.

## 2.6 | Blood and organ collection

To detect changes in alanine transaminase (ALT), the blood was collected (20–30 µl) from the tail vein 2–3 days before tamoxifen treatment for male and female mice. After initiation of tamoxifen therapy, blood was collected on Days 5–7 for female mice and on Days 5, 7, 9 and 11 for male mice. Animals were humanely euthanized by decapitation to collect tissues and organs for further study when ALT was above 200 IU in *Hmgcr*-KO animals. Accordingly, tissues were taken for female mice (KO and floxed) from 5 to 7 days after the start of tamoxifen therapy and for males from 7 to 11 days.

At the endpoint, the following samples were collected: plasma to study metabolomic and biochemical profile; liver for transcriptomic, metabolomic, biochemical, mitochondrial, gene expression and histological measurements; and skeletal muscles and brain tissue for mitochondrial and gene expression measurements.

## 2.7 | Liver transcriptome analysis

For RNA isolation, a QIAGEN AllPrep DNA/RNA/miRNA (QIAGEN, Germany) reagent kit was used. A 200 ng of isolated RNA was used for ribosomal RNA depletion with the MGIEasy rRNA Depletion Kit (MGI Tech Co., Ltd), followed by library preparation using the MGIEasy RNA Directional Library Prep Set (MGI Tech Co., Ltd) according to the manufacturer's instructions. The quality and quantity of the obtained libraries were evaluated with an Agilent 2100 Bioanalyzer system and a Qubit 2.0 fluorometer, respectively. Libraries were used as templates for DNB preparation, and sequencing was done with the DNBSEQ-G400RS sequencing platform, using the DNBSEQ-G400RS High-throughput Sequencing Set (PE 150) (MGI Tech Co., Ltd), to provide 150-bp paired-end sequencing reads (approximately 20 million reads per sample).

To determine the whole-transcriptome changes in female and male KO mice, we performed RNA-sequencing (RNA-seq). Whole-transcriptome RNA-seq reads were obtained using SOLiD 5500xl paired-end sequencing from Life Technologies. Preprocessing, quality control, read trimming and filtering were performed with *fastp* (Chen et al., 2018). Then, the reads were aligned to the mouse reference genome (GRCm39) and mapped back to the mouse transcriptome using the *Rsubread* package (Liao et al., 2019) on R software (Version 4.2.1). The differential gene expression analysis was performed with the *DESeq2* package (Love et al., 2014). Gene expression data from *Hmgcr*-KO samples with  $|\log_2FC| > 1$  and false discovery rate (FDR) *P*-adjusted <0.001 were considered as differentially expressed from the

floxed group. Enrichment analysis was performed using *clusterProfiler* (Wu et al., 2021) based on the Reactome database (<https://reactome.org/>) with the *ReactomePA* package and the Kyoto Encyclopedia of Genes and Genomes (KEGG) database (<https://www.genome.jp/kegg/>).

## 2.8 | Detection of endogenous metabolites in plasma and liver

Blood plasma and liver tissue were collected from animals and profiled using a commercially available MxP<sup>®</sup> Quant 500 kit, which detects 630 metabolites from 26 biochemical classes (BIOCRATES Life Sciences AG, Austria). After mice were decapitated, blood was collected in heparin-coated tubes and centrifuged at 1000 × *g* and 4°C for 10 min to obtain plasma. Frozen samples were sent to BIOCRATES Life Sciences AG. Data of all measured metabolites were used as received; no data correction was applied except for the exclusion of metabolite data under the level of detection. Further details regarding the methods used to conduct each assay are available at <https://biocrates.com/>. Metabolomic data were normalized using log transformation and 'Pareto scaling' and analysed with MetaboAnalyst 5.0 (Pang et al., 2021).

## 2.9 | Western blot analysis in liver homogenates

Liver tissues were homogenized (1:10 [w/v]) with a lysing buffer (containing 4-M urea, 140-mM Tris base, 1% SDS, 1% Igepal, Halt™ Protease and Phosphatase Inhibitor Cocktail and 1-mM dithiothreitol [DTT]) using an Omni Bead Ruptor 24 homogenizer (Omni International, Kennesaw, GA, USA). The total amount of protein in each sample was detected using the Lowry method. Each well of the Bolt™ 8% Bis-Tris Plus gel (Thermo Fisher Scientific, Waltham, MA, USA) was loaded with 20 µg of protein per sample. Following the manufacturer's instructions, a constant voltage (200 V) was used for electrophoresis. After electrophoresis, proteins were transferred to a polyvinylidene fluoride membrane (iBlot<sup>®</sup>2 PVDF Regular Stacks, Thermo Fisher Scientific, Waltham, MA, USA), which was blocked using 5% bovine serum albumin (BSA) dissolved in 1× Tris-buffered saline (TBS) for 1 h at room temperature. The membranes were incubated overnight with anti-HMGCR [EPR1685(N)] primary antibodies (Abcam Cat# ab174830, [RRID:AB\\_2749818](https://pubmed.ncbi.nlm.nih.gov/2749818/)) at 4°C. After incubation, the membranes were washed with TBS several times, and then the secondary antibodies (horseradish peroxidase [HRP]-linked anti-rabbit IgG antibodies diluted 1:50,000 [Cat# 7074, [RRID:AB\\_2099233](https://pubmed.ncbi.nlm.nih.gov/2099233/), Cell Signaling Technology, Danvers, MA, USA]) were added to the membrane for 1 h and then washed again with TBS. Mouse anti-actin Ab-5 C4 antibody diluted 1:4000 (Cat# 612656, Lot: 7033721, [RRID:AB\\_2289199](https://pubmed.ncbi.nlm.nih.gov/2289199/), BD Biosciences, San Jose, CA, USA) was used as house-keeping in combination with HRP-linked anti-mouse IgG antibody diluted 1:50,000 (Cat# 7076, [RRID:AB\\_330924](https://pubmed.ncbi.nlm.nih.gov/330924/), Cell Signaling Technology, Danvers, MA, USA).

The membranes were developed using SuperSignal™ West Pico PLUS Chemiluminescent Substrate (Thermo Fisher Scientific, Waltham, MA, USA). The images were captured with the Azure c600 system and analysed with AzureSpot 2.0 software (Azure Biosystems, Dublin, CA, USA).

## 2.10 | Quantitative PCR (qPCR) analysis

Total RNA from mouse liver tissue slices treated with 20- $\mu$ M palmitoylcarnitine for 2 h was isolated using TRI reagent (Sigma-Aldrich, Schnellendorf, Germany), and the High-Capacity cDNA Reverse Transcription Kit (Applied Biosystems™, Waltham, MA, USA) was used to synthesize a first-strand cDNA. qPCR analysis of gene expression was performed by adding SYBR® Green Master Mix (Applied Biosystems™) to each sample together with forward and reverse primers that are specific for glucose-6-phosphate isomerase 1 (GPI1), carnitine palmitoyltransferase 1a (CPT1A), acyl-coenzyme A oxidase 1 (ACOX1), pyruvate dehydrogenase kinase, **isoenzyme 4 (PDK4)**, peroxisome proliferator-activated receptor (PPAR) gamma coactivator-1 alpha (PGC1 $\alpha$ ), *Hmgcr* C-terminus coding mRNS (*Hmgcr*Ct) and *Hmgcr* N-terminus coding mRNS (*Hmgcr*Nt) primers were applied. Reactions were performed using Magnetic Induction Cycler (MIC) (Bio Molecular Systems, Queensland, Australia). According to the manufacturer's instructions, the reaction conditions were holding 50°C for 2 min and 95°C for 5 min, followed by 60 cycles of 95°C for 15 s, 60°C for 60 s and the analysis of the melt curve at the end (72–95°C, 0.3°C·s<sup>-1</sup> to ensure the specificity of the amplicon). The primer sequences are available in the [supporting information](#).

## 2.11 | Biochemistry assays

Biochemical parameter measurements were performed in plasma and liver homogenates. Measurements were carried out using commercially available kits according to the manufacturer's instructions. Reagent kits for cholesterol, triglycerides, glucose and ALT were purchased from Instrumentation Laboratory (Milan, Italy). The non-esterified fatty acid (NEFA) assay was performed using a kit from Wako Chemicals Europe GmbH (Neuss, Germany). For  $\beta$ -hydroxybutyrate measurements, a kit from BioSystems (Barcelona, Spain) was used. A reagent kit for the measurement of lactate was purchased from Roche Diagnostics (Mannheim, Germany). **Catalase** was quantified using enzymatic reactions with **hydrogen peroxide** (H<sub>2</sub>O<sub>2</sub>) and detected spectrophotometrically.

## 2.12 | Determination of acylcarnitine profile

Determination of the content of acylcarnitines and phytanoylcarnitine in mouse liver was performed by ultra-performance liquid chromatography–tandem mass spectrometry (UPLC/MS/MS) as described previously (Liepinsh et al., 2017) with some modifications.

The Waters Acquity UPLC H-Class chromatograph was coupled to the Waters Xevo TQ-S tandem mass spectrometer. Chromatographic separation was performed on the Waters Acquity UPLC BEH Hilic (2.1  $\times$  100 mm, 1.7  $\mu$ m) column in gradient mode. Solvent A was 10-mM ammonium acetate with 0.2% formic acid in water, and Solvent B was acetonitrile. The initial mobile phase composition was 10% Solvent A and was linearly increased to 20% Solvent A in 7 min. The total run time with column flush and re-equilibration was 10 min. The column temperature was 30°C, and the flow rate was 0.5 ml·min<sup>-1</sup>. Data acquisition was performed in positive electrospray ionization (ESI+) and multiple reaction monitoring (MRM) mode. The ion source parameters were as follows: source temperature of 120°C, capillary voltage of 2.5 kV, desolvation gas temperature of 600°C, and desolvation and cone gas flow of 800 and 150 L·h<sup>-1</sup>, respectively. Each compound was individually infused to obtain specific MRM transitions and cone/collision voltages.

The liver sample extraction was performed using homogenization in buffered KH<sub>2</sub>PO<sub>4</sub> solution (pH 4.9) with the following deproteinization by acetonitrile/methanol mixture and centrifugation steps (final weight-to-volume ratio 1:15). Supernatant was further diluted 25 times with acetonitrile/methanol 3:1 (v/v) and subjected to UPLC/MS/MS.

The concentrations of acylcarnitines were measured against a nine-point standard curve of C4–C18 and C2–C3 acylcarnitine in the range of 0.01–20 and 0.1–500 nM in the analytical sample, respectively. The concentration of phytanoylcarnitine was calculated using the C18 acylcarnitine standard.

## 2.13 | Mitochondrial functionality assessment

Mitochondrial respiration measurements were performed at 37°C using Oxygraph-2k (O2k; Oroboros Instruments, Innsbruck, Austria) with O2k-Fluo-Modules in MiRO5 medium (110-mM sucrose, 60-mM K-lactobionate, 0.5-mM EGTA, 3-mM MgCl<sub>2</sub>, 20-mM taurine, 10-mM KH<sub>2</sub>PO<sub>4</sub>, 20-mM HEPES, pH 7.1, 0.1% BSA essentially free of fatty acids and 20-mM creatine). All chemicals for MiRO5 were obtained from *Sigma-Aldrich* (Schnellendorf, Germany). Mitochondrial functionality was determined in liver tissue homogenates that were prepared using a Teflon-glass pestle at a concentration of 80 mg·ml<sup>-1</sup> with MiRO5 respiration medium.

Fatty acid oxidation (FAO)-dependent mitochondrial respiration at LEAK state was measured using 10- $\mu$ M palmitoylcarnitine and 0.5-mM **malate** as substrates (FAO–NADH [FN] pathway). **ADP** was added to a concentration of 5 mM to assess respiration in the OXPHOS state. **Pyruvate** and **glutamate** (5 and 10 mM; **NADH** [N] pathway) were then added to reconstitute FN pathway-linked respiration. **Succinate** (10 mM, S pathway) was added to reconstitute convergent FAO–NADH–succinate (FNS)-linked respiration. Afterward, titration with uncoupler carbonyl cyanide 3-chlorophenylhydrazone (CCCP) was performed in steps of 0.5  $\mu$ M to assess maximal electron transport system capacity (ET state). Then, rotenone (Rot) (0.5  $\mu$ M) and antimycin A (2.5  $\mu$ M) were added stepwise to determine the S-linked respiration

and residual oxygen consumption (ROX), respectively. All substrates and inhibitors were purchased from Sigma-Aldrich (Schnellendorf, Germany), except for ADP (Calbiochem, San Diego, CA, USA).

For determination of the contribution of each substrate to the respiratory rate, the flux control efficiency ( $J_{Z-\gamma}$ ) was calculated (Equation 1) according to

$$J_{Z-\gamma} = 1 - Y_X/Z_X \quad (1)$$

where  $Z_X$  is the reference state with high (stimulated or un-inhibited) flux and  $Y_X$  is the background state at low flux, upon which the metabolic control variable,  $X$ , acts.

## 2.14 | Histology

Liver samples were embedded in an optimal cutting temperature compound (Tissue-Tek<sup>®</sup> O.C.T.<sup>™</sup> Compound, Sakura Finetek Europe B.V., Alphen aan den Rijn, The Netherlands) and frozen by placing in a dry ice/isopropanol slurry. Frozen samples were stored at  $-20^\circ\text{C}$ ; 10- $\mu\text{m}$ -thick liver sections were obtained by cutting samples using a Thermo Scientific<sup>™</sup> HM525 NX Cryostat (Thermo Scientific, Waltham, MA, USA). Slides with sections on Superfrost Plus microscope slides (Thermo Scientific, Waltham, MA, USA) were stored at  $-20^\circ\text{C}$  until staining was performed.

## 2.15 | Haematoxylin and eosin staining

Liver sections were fixed for 10 min in 96% ethanol. Dried sections were washed 3–4 times with tap water and stained in Mayer's hemalum solution (MilliporeSigma, Burlington, MA, USA) for 2 min. Slides were washed several times ( $5 \times 2$  min) in warm tap water. To remove excess stain and define nuclei following haematoxylin staining, slides were dipped in acid alcohol (0.5% HCl in 70% ethanol) and washed in tap water for 5 min. Cytoplasm was stained after dipping slides several times in 0.25% Eosin Y aqueous solution (Gentaur, Kampenhout, Belgium). Stained sections were washed in tap water, dried, cleared in xylene and coverslipped using DPX mounting medium (Sigma-Aldrich, St. Louis, MO, USA). Images were taken with a Leica DMI8 inverted light microscope (Leica Microsystems, Wetzlar, Germany) using a Leica HC PL APO 10 $\times$ /0.45 objective.

## 2.16 | Immunohistochemistry

The Immuno-related procedures used comply with the recommendations made by the *British Journal of Pharmacology*. Staining of mouse liver sections was performed based on the Guide to STED Sample Preparation (Leica, Germany). Endogenous peroxidase blocking with 0.3%  $\text{H}_2\text{O}_2$  was performed after tissue fixation with 4% paraformaldehyde solution. The following primary antibodies were used in this study: rabbit anti-catalase antibody (1:100; #ab209211, RRID:AB\_

3086611, Abcam, Cambridge, UK) and rabbit anti-TOM20 antibody (1:200; #42406, RRID:AB\_2687663, Cell Signaling Technology, Danvers, MA, USA). Goat anti-mouse IgG Abberior STAR RED antibody (1:200; #STRED-1001-500UG, RRID:AB\_3068620, Abberior Instruments, Göttingen, Germany) was used as a secondary antibody. Nuclei were stained using DAPI Solution (#62248, Thermo Fisher Scientific, Waltham, MA, USA). Samples were coverslipped using ProLong Gold Antifade Mountant (#P36930, Thermo Fisher Scientific, Waltham, MA, USA). Negative controls, replacing the primary antibody with a buffer solution only, were performed to evaluate the background staining. Imaging was performed on a Leica Stellaris 8 confocal microscope (Leica Microsystems, Wetzlar, Germany) using a Leica HC PL APO 93 $\times$ /1.30 GLYC motCORR objective.

## 2.17 | Transmission electron microscopy (TEM)

The liver specimens were cut into 1-mm<sup>3</sup> tissue blocks and further processed for TEM using conventional protocols. According to routine laboratory procedures, the samples were fixed in 2.5% glutaraldehyde (#16400, Electron Microscopy Sciences, Thermo Fisher Scientific, Waltham, MA, USA) in 0.1-M phosphate buffer with 2.3-M sucrose, pH 7.2, for 4 h at  $4^\circ\text{C}$  and then washed several times with a 0.1-M phosphate buffer solution at  $4^\circ\text{C}$ . Subsequently, the samples were postfixed in 1% osmium tetroxide (#19110, Electron Microscopy Sciences, Thermo Fisher Scientific, Waltham, MA, USA) for 1 h at  $4^\circ\text{C}$  and washed again with the 0.1-M phosphate buffer solution at  $4^\circ\text{C}$ . Afterward, the samples underwent dehydration in graded concentrations of ethanol, were stained *en block* with a 2% alcoholic uranyl acetate solution at  $4^\circ\text{C}$  and were gradually embedded in epoxy resin (#14120, Electron Microscopy Sciences, Thermo Fisher Scientific, Waltham, MA, USA) using Beam capsules. Following the completion of block polymerization at  $60^\circ\text{C}$  for 24 h, semi-thin sections were cut from the blocks with a glass knife to select the appropriate region for thinning. Ultrathin 60-nm-thick sections were cut with an ultra  $45^\circ$  2.00-mm diamond knife (#DU 4520, Diatome, Science Services, Germany) using an RMC Boeckeler PowerTome PC ultramicrotome (#R75840, RMC Boeckeler, Tucson, AZ, USA). The sections were then collected on Formvar-coated 200-mesh copper grids (#930245, Sigma-Aldrich, Merck KGaA, Darmstadt, Germany) and double stained with 2% uranyl acetate (#22400-2, Electron Microscopy Sciences, Thermo Fisher Scientific, Waltham, MA, USA) and lead citrate (#15326, Sigma-Aldrich, Merck KGaA, Darmstadt, Germany). Finally, the sections were examined with a JEM 1011 transmission electron microscope (JEOL, Japan) at magnifications ranging from  $\times 3000$  to  $\times 20,000$  and captured at a magnification of  $\times 8000$ .

## 2.18 | Materials

Details of materials and suppliers are provided in specific subsections in Methods.

## 2.19 | Statistical analysis

The data and statistical analysis comply with the recommendations of the *British Journal of Pharmacology* on experimental design and analysis in pharmacology (Curtis et al., 2022). Statistical analysis was performed using GraphPad Prism (GraphPad Software, Inc., La Jolla, CA, USA). Two-way analysis of variance (ANOVA) or mixed-effects models were used to detect multiple factors. Šidák's or Fisher's multiple comparisons tests were used. Differences between two groups were assessed using Student's *t*-test. *P* values less than 0.05 were considered significant. Data are shown as mean ± SEM.

## 2.20 | Nomenclature of targets and ligands

Key protein targets and ligands in this article are hyperlinked to corresponding entries in <https://www.guidetopharmacology.org> and are permanently archived in the Concise Guide to PHARMACOLOGY 2021/22 (Alexander et al., 2021).

# 3 | RESULTS

## 3.1 | *Hmgcr* gene KO is induced in the liver

*Hmgcr*-KO was induced by feeding *Hmgcr*<sup>LoxP/LoxP</sup>-*Rosa26*<sup>Cre/WT</sup> mice with tamoxifen-supplemented chow for 5 days and compared with tamoxifen-treated *Hmgcr*<sup>LoxP/LoxP</sup>-*Rosa26*<sup>WT/WT</sup> (floxed) mice (Figure S1). During a tamoxifen treatment, food intake and body weight were both decreased in the *Hmgcr*-KO and floxed mouse groups (Figure 1a,b). After being subsequently fed with a regular chow diet, food intake increased in the floxed and *Hmgcr*-KO groups to the same levels (Figure 1b). In *Hmgcr*-KO animals, 5-day treatment with a low dose of tamoxifen (14 mg·kg<sup>-1</sup> with chow) was sufficient to induce gene KO that resulted in the acquisition of a profoundly negative phenotype within a few days after the cessation of the tamoxifen treatment. We observed acute liver failure, but no changes in other tissues (HMGR expression and organ-specific phenotype). The liver is likely to be the most negatively affected by this treatment because of the high bioavailability and high metabolism rate of tamoxifen in this organ. Notably, the early onset of liver damage in the model may be a limiting factor for the induction of *Hmgcr*-KO in other tissues.

To determine the extent of liver damage caused by *Hmgcr*-KO, we first confirmed that *Hmgcr* was effectively abrogated by tamoxifen treatment in our model, which we accomplished by performing PCR analysis. In female *Hmgcr*-KO mice, the average mRNA levels of carboxyl (C)-terminal and amino (N)-terminal *Hmgcr* fragments were significantly reduced by as much as sixfold (Figure 1c,d). This reduction resulted in about a 50% decrease in HMGR protein levels. In male *Hmgcr*-KO mice, the average *Hmgcr* mRNA level was about threefold lower than in floxed mice. In addition, a decrease in *Hmgcr* protein content in female liver samples was confirmed by western blot analysis (Figure 1e). Because *Hmgcr* is a rate-limiting step in cholesterol

synthesis, changes in the cholesterol biosynthesis rate might be expected in *Hmgcr*-KO animals; however, shortly after *Hmgcr* was knocked out, the cholesterol concentration in plasma was decreased only by 39% in females, whereas the plasma cholesterol level in males was not (Figure 1f). In addition, the level of cholesteryl ester, the storage form of cholesterol, in the liver of female and male *Hmgcr*-KO mice was 30%–60% lower than in floxed female and male mice (Figure 1h). Thus, neither cholesterol nor cholesteryl ester levels were depleted at the humane endpoint of the experiment (Figure 1f,g).

## 3.2 | KO mice develop lethal liver failure

The rapid onset of acute liver failure was observed in both female and male *Hmgcr*-KO mice. The lethal phenotype manifested on Days 6–8 in females and on Days 9–11 in males (Figure 2a). The humane endpoints were determined based on clinical observations (general weakness, immobility and reduced body temperature) and ALT plasma concentration as a marker of liver damage. In female mice, plasma ALT concentrations 7 days after tamoxifen treatment was initiated (female endpoint) reached 600 U·L<sup>-1</sup>. In male mice, the onset of liver damage (male endpoint) was observed approximately 3 days after observed in female mice (Figure 2b). In contrast, in the *Rosa26*<sup>Cre</sup> or floxed animals, three cycles of tamoxifen treatment (5 days of treatment + 2 days of normal chow for each treatment) did not induce any changes in liver function. Liver weight in the female *Hmgcr*-KO mice was significantly increased, from 1.0 ± 0.1 to 1.4 ± 0.4 g. Liver damage was confirmed by macroscopic observation of the liver and histological assays (Figure 2c,d), through which pale patches in the liver or a pale colour across the whole liver were observed. The histological analysis also revealed profoundly affected regions in liver tissue adjacent to unaffected cells. This variability in *Hmgcr*-KO-induced effects indicated that not all liver cells were affected simultaneously. Large-scale liver cell death due to apoptosis, necrosis, cell hypertrophy, microvesicular lipidosis and cystic degeneration was observed via a histological analysis of liver slices obtained from *Hmgcr*-KO mice. After 5 days of tamoxifen treatment, the *Hmgcr*-KO mouse liver histology was unchanged (Figure S2a). At the endpoint, no macroscopic change or obvious cell damage was observed in non-liver tissues in either female or male *Hmgcr*-KO mice. Levels of a muscle damage biomarker (creatinine kinase) and a marker of kidney damage (blood urea) were unchanged in the *Hmgcr*-KO mice.

## 3.3 | Blood and liver biochemical analyses reveal a systemic energy metabolism crisis

In addition to liver damage markers, we measured the levels of biochemical markers in plasma and liver to evaluate changes in fatty acid and glucose metabolism at the experiment endpoint, to understand the effect of *Hmgcr*-KO on the liver and whole body. NEFA concentrations were increased in *Hmgcr*-KO mouse liver and plasma by 30%

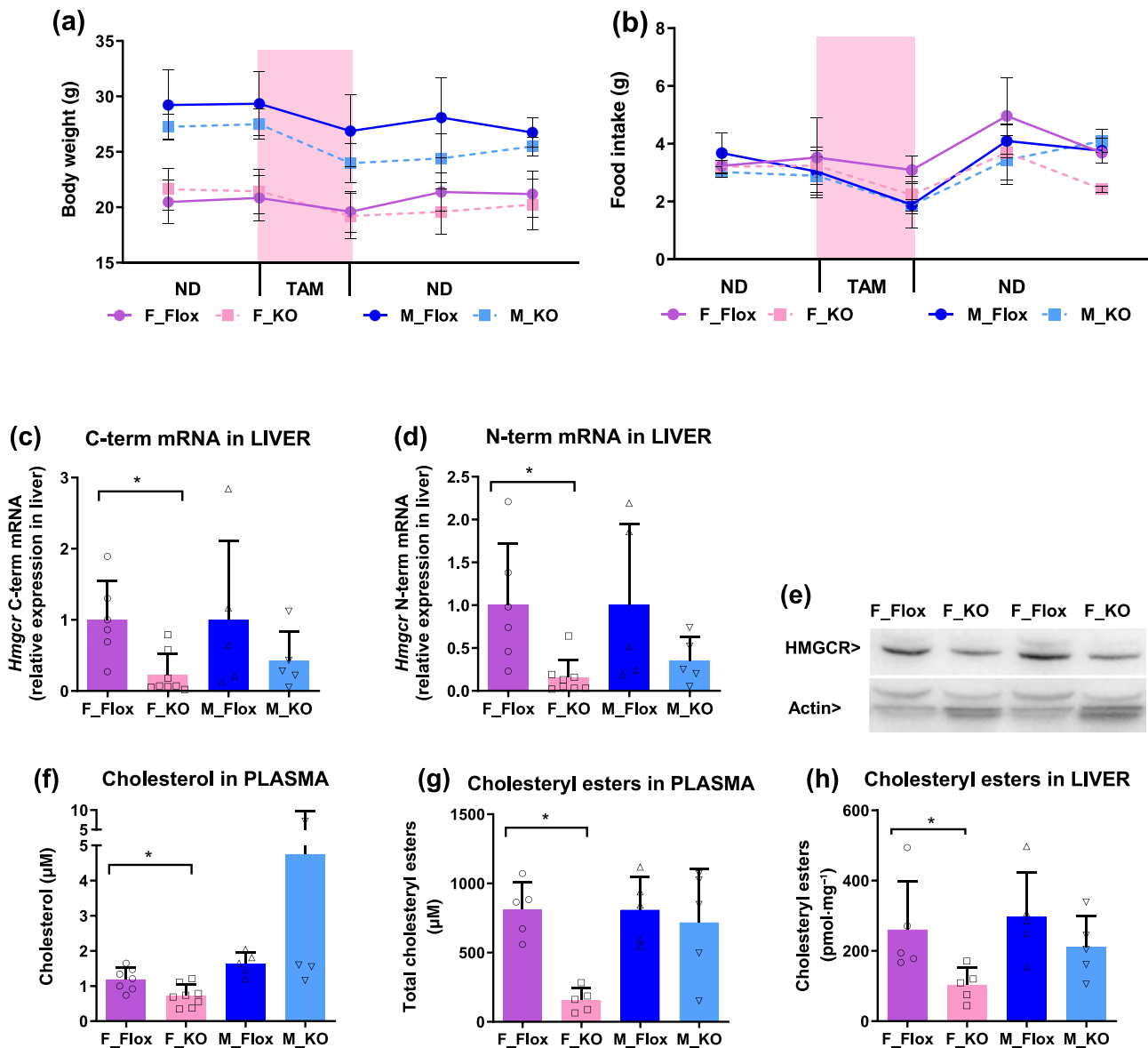


**FIGURE 1** Tamoxifen treatment induced lower expression of *Hmgcr*. (a, b) Tamoxifen-containing chow intake was slightly lower, thus inducing a temporary decrease in the body weight of floxed and knockout (KO) mice. (c, d) Gene KO was confirmed by a decrease in *Hmgcr* mRNA levels of C-terminal and N-terminal fragments and (e) *Hmgcr* protein content in the liver of KO animals. (f–h) A deficiency of *Hmgcr* protein led to a decreased content of cholesterol and cholesteryl esters in the plasma and liver. Plasma and liver tissue samples were collected from floxed and KO male and female mice at the endpoint (Days 7–10). Data are shown as the mean  $\pm$  SEM ( $n = 5$ –8 mice per group). \* $P < 0.05$ , versus the corresponding sex of floxed mice, one-way analysis of variance (ANOVA) followed by unpaired  $t$ -test post hoc analysis. C-term mRNA, carboxyl-terminus of messenger ribonucleic acid; F\_Flox, floxed female; F\_KO, knockout female; M\_Flox, floxed male; M\_KO, knockout male; ND, normal diet; N-term mRNA, amino-terminus of messenger ribonucleic acid; TAM, tamoxifen diet.

and 200%, respectively, suggesting a decreased capability of the liver to metabolize fatty acids (Figure 2e,f). This finding was in line with the observation indicating that the triglyceride content in the liver was increased from 7-fold to 13-fold (Figure 2g). Under fasting conditions, the liver plays a major role in generating and supplying glucose to the circulatory system to maintain the functions of glucose-dependent tissues such as the brain. In *Hmgcr*-KO mice, we did not observe significantly lower food intake (Figure 1b), indicating that changes in liver biochemistry, not the fasting status, affected the levels of glucose and

fatty acids in plasma. Lower hexose and lactate contents were observed in the livers of the *Hmgcr*-KO mice, suggesting increased carbohydrate utilization in the liver as a reason for reduced systemic glucose availability (Figure 2i,j). The glucose concentration in *Hmgcr*-KO mouse plasma was significantly lower than in floxed mouse plasma (Figure 2k). In four out of eight female *Hmgcr*-KO mice, the glucose concentration was less than 5 mM (1.5–4.5 mM), suggesting that changes in liver fat and the carbohydrate metabolism-induced hypoglycaemia observed at the humane endpoint contributed to the

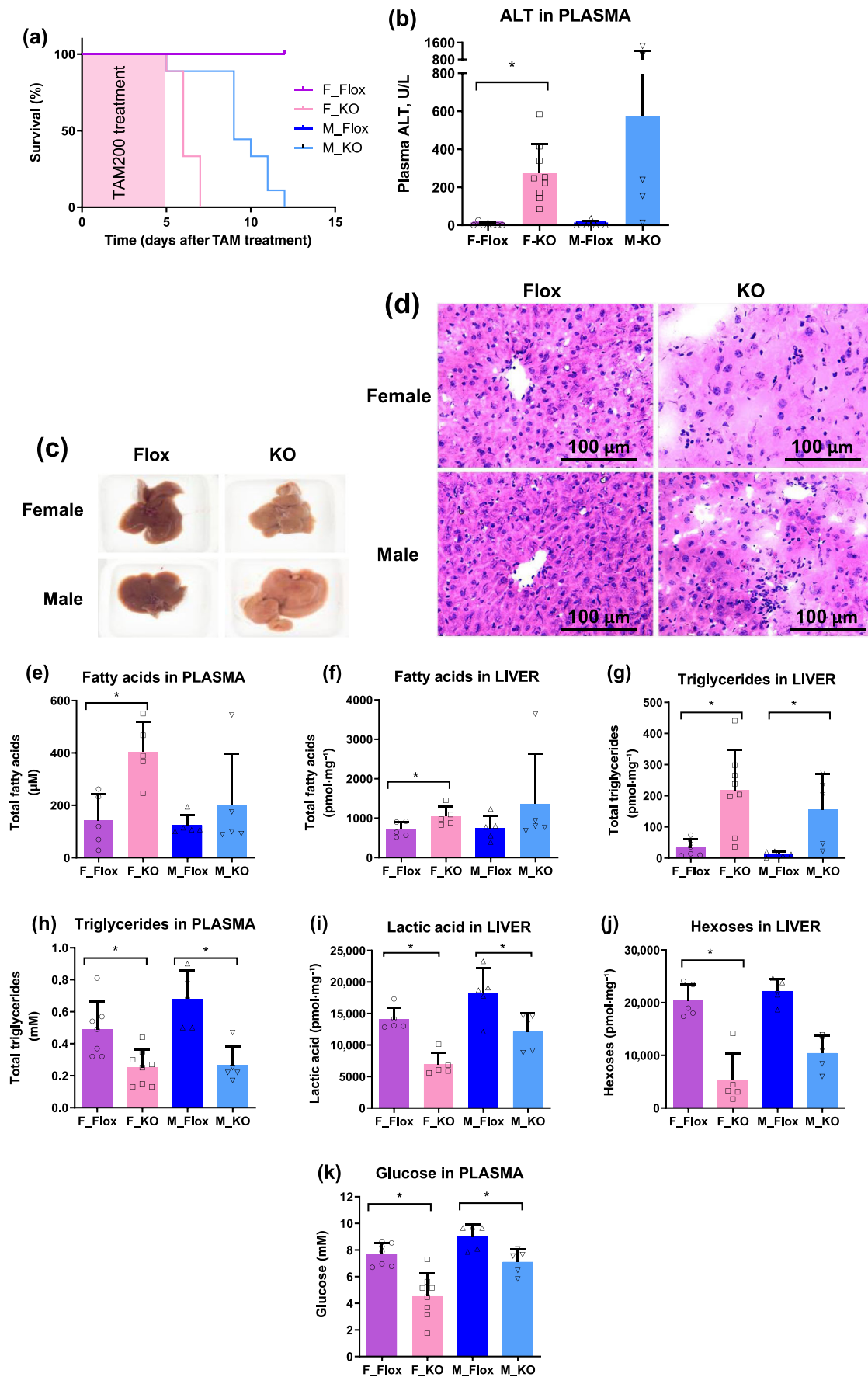


**FIGURE 2** Legend on next page.

lethality of *Hmgcr*-KO mice. The levels of biochemical markers in plasma and liver were not changed in *Hmgcr*-KO mice on Day 5 (Figure S2). Overall, the analysis of biochemical marker levels in plasma and liver pointed to marked changes in fatty acid and glucose metabolism in the liver that led to a systemic energy metabolism crisis in glucose-dependent tissues.

### 3.4 | Transcriptomic analysis reveals changes in energy metabolism pathway activity

Further changes in energy metabolism signalling pathways were explored by transcriptome analysis. Whole-transcriptome RNA-seq reads showed marked changes in the *Hmgcr*-KO mouse transcriptome (Figures 3a and S3a). A principal component analysis (PCA) revealed that clusters of *Hmgcr*-KO samples were separate from the other samples, indicating that *Hmgcr* was the main factor driving liver transcriptome changes in male and female mice (Figure S3c). Overall, in female mouse liver, the expression of 3159 genes was up-regulated and that of 2470 genes was down-regulated ( $P < 0.001$ , fold change  $> 2$ ). Compared with female *Hmgcr*-KO mice, male *Hmgcr*-KO mice exhibited fewer changes in gene expression (Figure 3b and S3a). A Reactome enrichment analysis revealed that the activation levels of several pathways were significantly changed in female mice, and the expression of target genes related to lipid and fatty acid metabolism in mitochondria and peroxisomes was down-regulated (Figures 3c and S3d-f). All these findings indicated alterations to energy metabolism pathway activity.

In the liver, the activation of PGC1 $\alpha$  and PPAR gamma coactivator-1 beta (PGC1 $\beta$ ) facilitates organism adaptation to fasting, and these effects are mediated via several metabolic modifications, including those involved in the activation of mitochondrial metabolism, gluconeogenesis, FAO, ketogenesis and bile acid homeostasis (Besse-Patin et al., 2019; Piccinin et al., 2019). PGC1 $\alpha$  is involved in the activation of several transcription factors that regulate oxidative metabolism; these transcription factors include PPAR $\alpha$  and PPAR $\delta$ , forkhead box protein O1 (FOXO1), nuclear respiratory factors (Nrf1 and Nrf2) and the lipogenic regulator carbohydrate-responsive element-binding protein (ChREBP) (Chambers et al., 2013; Puigserver et al., 2003; Vega et al., 2000; Wu et al., 1999). In the *Hmgcr*-KO mice, only the expression of the PPAR $\alpha$  target genes was significantly down-regulated (Figure S3f), whereas FOXO1 and ChREBP target

genes were not affected. The expression of Nrf pathway genes was significantly up-regulated in *Hmgcr*-KO mouse liver. Because lower PGC1 $\alpha$ /PPAR $\alpha$  target gene expression was found in *Hmgcr*-KO mice that had low glucose and high fatty acid levels (Figure 2), we can conclude that PPAR $\alpha$  transcriptional activity was specifically disrupted in *Hmgcr*-KO mouse liver.

The progressive form of fatty liver disease, such as nonalcoholic steatohepatitis (NASH), is to a large extent triggered by hepatic inflammation (Schuster et al., 2018). In *Hmgcr*-KO mice, despite high lipid levels and large areas of tissue damage, the expression of inflammatory marker genes such as tumour necrosis factor- $\alpha$  (TNF- $\alpha$ ), interleukin-1 $\beta$  (IL-1 $\beta$ ), IL-6 and inducible nitric oxide synthase (iNOS) was not increased. These findings were in line with the observation of nominal leukocyte infiltration, as assessed via liver histology (Figure 2d). In summary, in *Hmgcr*-KO mice, liver damage was not characterized by an inflammatory NASH-like pathophysiology profile.

### 3.5 | Metabolomic analysis points to changes in mitochondrial and peroxisomal pathway activity

For the identification of changes in liver energy metabolism, we performed metabolomic analysis in plasma and liver samples and found substantial differences in metabolite concentrations between floxed and *Hmgcr*-KO mice. The abundance of 69 and 175 of 551 metabolites changed ( $|\log_2FC| > 1$ ,  $P < 0.01$ ) in the liver and plasma of female *Hmgcr*-KO mice, respectively. In total, the abundance of 58 liver metabolites increased, and that of only 11 metabolites decreased (Figure 3e). As indicated by a PCA, the metabolic profiles of male and female floxed mice completely overlapped. The PCA score cluster of the female *Hmgcr*-KO mouse liver was completely separated from the other clusters, while the male *Hmgcr*-KO mouse liver metabolic profile overlapped with that of the KO female and floxed mice (Figure 3d). Thus, the metabolic phenotype was substantially different in *Hmgcr*-KO and floxed female mice, but greater variability was observed in *Hmgcr*-KO males. A similar pattern was observed in the transcriptomic and biochemical analysis data in male and female mice. The metabolomics analysis revealed changes in carbohydrate, lipid and amino acid metabolic pathways (Figure 3e,f). Fatty acids and their metabolism intermediates, namely, LC acylcarnitines, accumulated at substantially high levels, suggesting

**FIGURE 2** *Hmgcr* deletion induced acute lethal liver failure and disbalance in glucose and fatty acid turnover. (a) According to the Kaplan–Meier plot, a few days after the induction of *Hmgcr*-knockout (KO), mice reached the humane endpoint. (b) Acute liver failure was diagnosed by a substantial increase in plasma alanine transaminase (ALT) levels. (c) Liver damage in KO mice was confirmed by the macroscopic appearance of a pale liver. (d) The histological analysis of haematoxylin and eosin-stained sections revealed liver cell death. (e, f) Significantly increased concentrations of fatty acids in KO mouse liver and plasma suggest that liver metabolism shifted towards glucose utilization. (g) In KO mice, liver excess of fatty acids is converted into triglycerides, causing hepatic steatosis. (h) Lipid export from the liver is decreased and results in the low plasma triglyceride concentrations observed. (i) Lower content of lactate and (j) depleted hexoses in the KO mouse liver were observed. (k) Low glucose concentration in plasma suggests elevated carbohydrate utilization in the KO mice liver, causing systemic hypoglycaemia. Plasma and liver tissue samples were collected from floxed and KO male and female mice at the endpoint (Days 7–10). Data are shown as the mean  $\pm$  SEM ( $n = 5–8$  mice per group). \* $P < 0.05$ , versus the corresponding sex of floxed mice, one-way analysis of variance (ANOVA) followed by unpaired  $t$ -test post hoc analysis. F\_Floxed, floxed female; F\_KO, knockout female; M\_Floxed, floxed male; M\_KO, knockout male; TAM, tamoxifen.

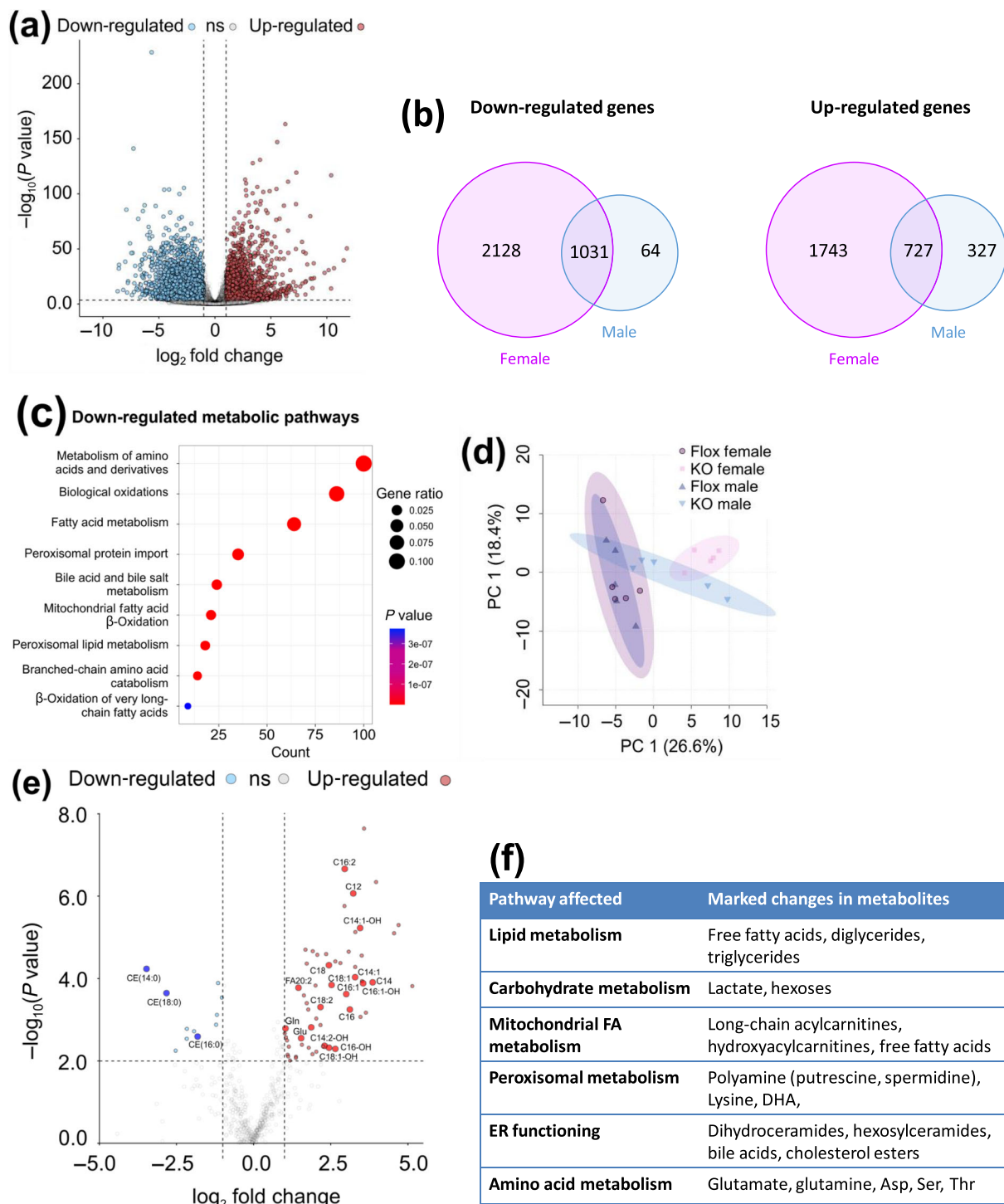


**FIGURE 3** Legend on next page.

disrupted mitochondrial and peroxisomal functionality. In the metabolomic data, 15 of the 59 metabolites with the greatest increase in abundance were LC acylcarnitines (Figure 3e). In addition, disruptions to the polyamine, bile acid, ceramide and glutamate/glutamine profiles were observed, indicating changes in peroxisomal and ER metabolism (Figure 3f). Overall, the metabolomic analysis revealed significantly changed mitochondrial and peroxisomal fatty acid metabolism.

### 3.6 | Mitochondrial dysfunction

A transcriptome pathway analysis revealed significant differences in the expression of metabolism-related genes in *Hmgcr*-KO mouse liver. Through a detailed analysis of these genes, we found significantly down-regulated expression by twofold to threefold of mitochondrial genes related to mitochondrial FAO (Figure 4a). These genes included those involved in fatty acid transport, acyl-CoA and acylcarnitine synthesis and most of the  $\beta$ -oxidation enzymes (Figure S3d). Similarly, lower expression of genes related to glutamate metabolism was observed in the *Hmgcr*-KO mouse liver. Overall, compared with male *Hmgcr*-KO mice, female *Hmgcr*-KO mice presented substantially lower mitochondrial metabolism-related gene expression.

Immunohistochemical (IHC) TOM20 staining, for a marker of mitochondrial mass and metabolic activity, revealed regional and time-dependent differences in the *Hmgcr*-KO mouse liver (Figures 4b and S4b). At the endpoint, most liver cells had lost TOM20-positive mitochondria, while there were a few other liver regions still carrying a significant number of TOM20-positive mitochondria (Figure 4b). In addition, the mitochondria in the *Hmgcr*-KO animals were smaller and had lost connection with each other. The early loss of mitochondria in female *Hmgcr*-KO mouse liver was observed as early as 5 days after the tamoxifen treatment was initiated (Figure S4b). Overall, the IHC findings indicated the presence of highly dysfunctional mitochondria in the *Hmgcr*-KO mouse liver.

Following IHC analysis, we evaluated whether changes in liver metabolism are related to disrupted mitochondrial function. High-resolution respirometry measurements showed that the mitochondrial respiration rate was markedly lower in female *Hmgcr*-KO mouse liver homogenate. At the endpoint in female and male *Hmgcr*-KO mice, the

mitochondrial FAO rate (with palmitoylcarnitine as a substrate) was significantly decreased by twofold to threefold (Figure 4d). A similar decrease in the mitochondrial respiration rate was observed in the FN and FNS pathways, suggesting that other pathways did not compensate for the reduced FAO in *Hmgcr*-KO mice that led to severe cellular energy deficiency (Figure 4d). The calculated flux control efficiency indicated that the electron transfer system in the *Hmgcr*-KO mouse liver was not disrupted. Therefore, it is likely that some mitochondria were dysfunctional while other mitochondria were functioning efficiently. A lowered FAO rate was observed in experiments with mitochondria from male *Hmgcr*-KO mouse liver, but this reduction in FAO rate was compensated by FNS pathway activity (Figure 4d). On Day 5, mitochondrial FAO was reduced only in female *Hmgcr*-KO mouse liver, and this was sufficiently compensated by other pathways (Figure S4a). Overall, the mitochondrial respiration measurements were in line with IHC findings, which indicated the presence of highly dysfunctional mitochondria and functional organelles in *Hmgcr*-KO mouse liver homogenate at the endpoint, with mitochondria relatively less affected by *Hmgcr*-KO on Day 5. Because no other changes were apparent on Day 5, the dysfunctional mitochondrial FAO could be considered the main point initiating all detrimental changes that were observed in *Hmgcr*-KO mice several days later.

### 3.7 | Altered ultrastructural appearance of mitochondria, ER and peroxisomes

Liver damage was confirmed through electron microscopic examination of *Hmgcr*-KO mouse liver samples, aligning with the previously mentioned gross anatomy and routine histopathological findings. Nevertheless, a characteristic feature observed in *Hmgcr*-KO mice was the heterogeneity in the alteration of hepatocytes.

Ultrastructural analysis of hepatocyte organelles revealed the alteration of reactive cytoplasmic organelles, primarily mitochondria, ER, peroxisomes and lysosomes, as confirmed in *Hmgcr*-KO mouse livers. Mitochondria in hepatocytes from *Hmgcr*-KO mouse liver appeared to vary greatly in size and shape (Figure 4c and S4c). The organelles mostly exhibited smooth outlines, and the intermembrane space was not enlarged. The orientation of cristae varied, and some

**FIGURE 3** Transcriptomic and metabolomic analysis revealed alterations in fatty acid metabolism in the liver mitochondria and peroxisomes of *Hmgcr*-knockout (KO) mice. (a) The volcano plot shows many statistically significant changes in female KO mice liver transcriptome. (b) A significant number of liver metabolism genes were affected in the transcriptome of KO mouse liver. (c) Reactome enrichment analysis of the differentially expressed genes in female floxed and KO mice livers. (d) Score plots of principal component analysis (PCA)-discriminated metabolites in the liver between the floxed and *Hmgcr*-KO male and female groups. (e) In the volcano plot of metabolomics data (floxed vs. KO female mice liver), long-chain (C12–C18:2) and hydroxylated (C14:2-OH–C18:1-OH) acylcarnitines stand out as the most increased metabolites and cholesterol esters (C14–C22:6) as a group of decreased metabolites. (f) Metabolomic analysis revealed the main metabolism pathways that were affected in the liver of KO mice. Liver tissue samples were collected from floxed and KO male and female mice ( $n = 5–8$  mice per group) at the endpoint (Days 7–10). Threshold values for significantly up-regulated and down-regulated genes are  $|\log_2FC| > 1$  and  $P$ -adjusted  $< 0.001$  in the RNA-sequencing (RNA-seq) analysis of *Hmgcr*-KO mouse liver compared with floxed mice. Volcano plots of metabolomes show statistical significance ( $P$  value  $< 0.05$ ) versus the magnitude of fold change ( $FC > 2.0$ ) in floxed and KO female mice livers. Differential expression analysis was performed on a total of 27,821 genes using R software (Version 4.2.1) with the *DESeq2* package. Metabolomic analyses were produced using MetaboAnalyst 5.0.

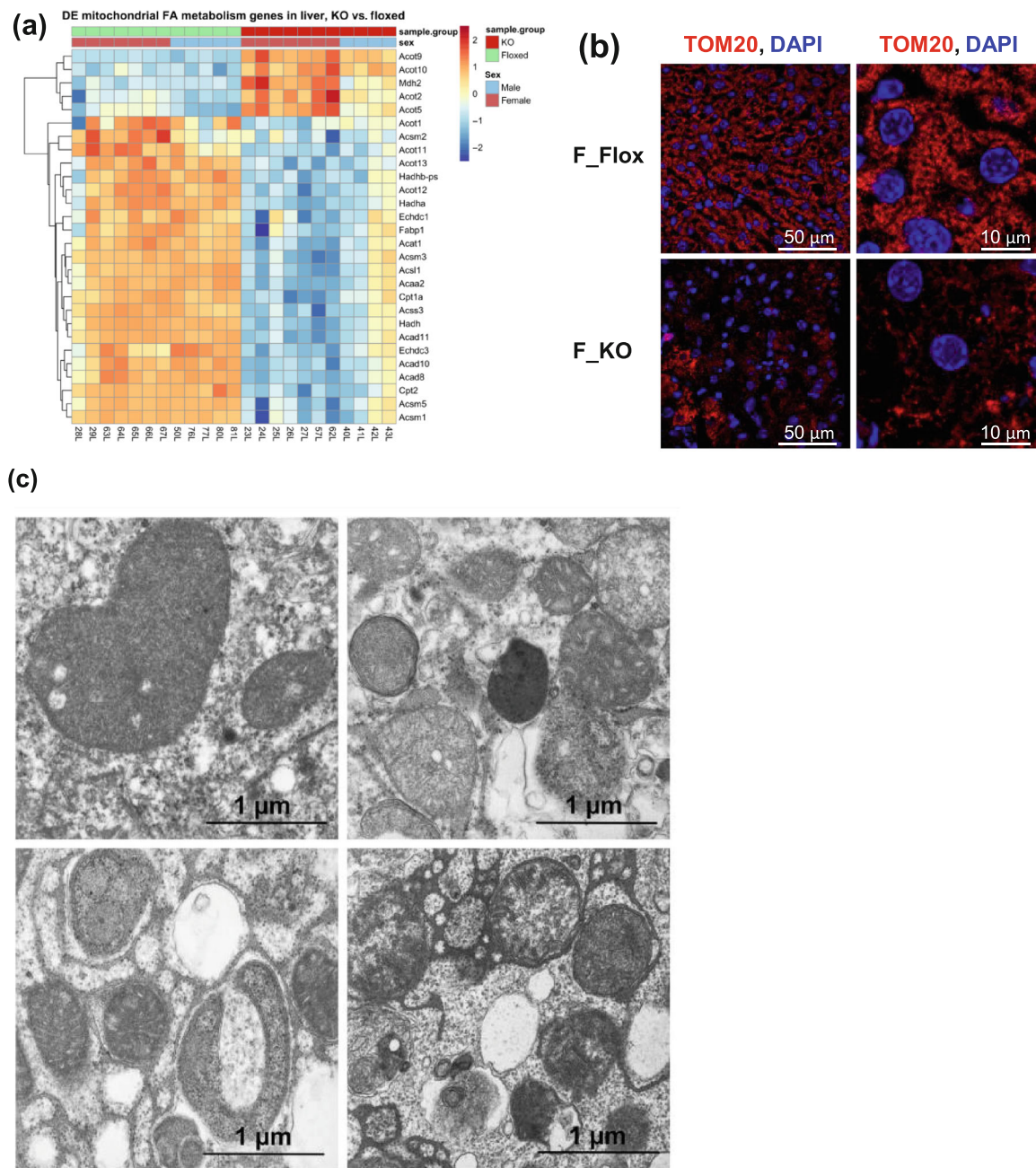


**FIGURE 4** Mitochondrial function is markedly decreased in *Hmgcr*-knockout (KO) mice. (a) Many genes related to mitochondrial fatty acid metabolism are decreased in KO animal liver. (b) The number of TOM20-positive mitochondria is reduced in KO mice. (c) Hepatocyte mitochondrial involvement and heterogeneity of appearance were confirmed in both male and female KO mice liver at the ultrastructural level. (d) High-resolution respirometry shows a significantly lower mitochondrial respiration rate on palmitoylcarnitine (fatty acid oxidation [FAO]) and other substrates. (e, f) The content of short- and medium-chain acylcarnitines is not changed. (g, h) Long-chain acylcarnitines and (i) long-chain 3-hydroxy-acylcarnitines are substantially increased in KO mice livers reaching a very high total long-chain acylcarnitine level. (j) Glutamic acid levels in female and male KO mice livers were significantly higher. Liver tissue and plasma samples were collected from floxed and KO male and female mice at the endpoint (Days 7–10). Data are shown as the mean  $\pm$  SEM ( $n = 5–8$  mice per group). \* $P < 0.05$ , versus the corresponding sex of floxed mice, one-way analysis of variance (ANOVA) followed by unpaired  $t$ -test post hoc analysis. AC, acylcarnitines; AmA, antimycin A; C14:1, tetradecenoylcarnitine; C14:1-OH, hydroxytetradecenoylcarnitine; C14:2-OH, hydroxytetradecadienoylcarnitine; C16, hexadecenoylcarnitine; C16:1, hexadecenoylcarnitine; C16:1-OH, hydroxyhexadecenoylcarnitine; C16:2, hexadecadienoylcarnitine; C16:2-OH, hydroxyhexadecadienoylcarnitine; C16-OH, hydroxyhexadecanoylcarnitine; C18, octadecenoylcarnitine; C18:1, octadecenoylcarnitine; C18:1-OH, hydroxyoctadecenoylcarnitine; C18:2, octadecadienoylcarnitine; DAPI, 4',6'-diamidino-2-phenylindole, a nuclear staining dye; F, FAO-dependent pathway; F\_Floxed, floxed female; F\_KO, knockout female; FA, fatty acids; G, glutamate; LEAK<sub>N</sub>, substrate metabolism-dependent state without adenylates; M\_Floxed, floxed male; M\_KO, knockout male; N, NADH pathway; OXPHOS, oxidative phosphorylation-dependent state; P, pyruvate; PC, palmitoylcarnitine; Rot, rotenone; ROX, residual oxygen consumption; S, succinate; S, succinate pathway; TOM20, staining dye for the mitochondrial import receptor subunit TOM20; U, uncoupler carbonyl cyanide 3-chlorophenylhydrazone.

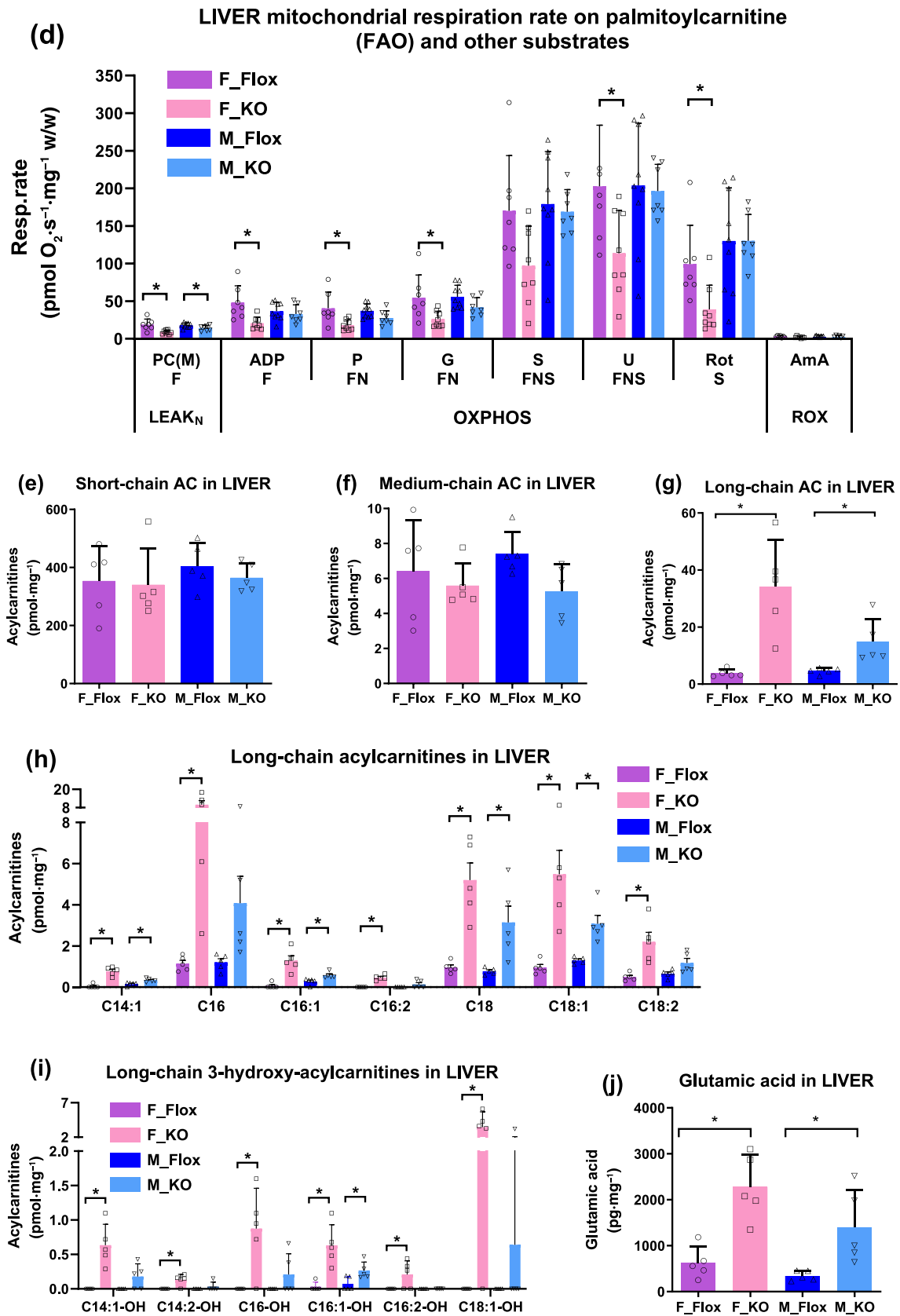


FIGURE 4 (Continued)

were curved. Certain cristae displayed varying degrees of vacuolation, and the number of cristae was reduced. The predominant electron optical density of the mitochondrial matrix was moderate; however, some organelles exhibited a low density of the mitochondrial matrix. Notably, enhanced mitochondrial autophagy contributes to autophagosome and pseudo-myelin figure formation. The latter were found both intracellularly and extracellularly.

Rounded or oval and mostly small-sized structures, commonly referred to as microperoxisomes, were found in markedly reduced numbers in both *Hmgcr*-KO male and female hepatocytes, indicating an association with the reduction of catalase activity. A moderately electron-dense, granular matrix, a mostly non-crystalloid core and the absence of a nucleoid were characteristics of peroxisomes. Additionally, the disappearance of properly arranged stacks of rough ER cisternae, contributing to the formation of ergastoplasm and ensuring sufficiency in peroxisome enzyme synthesis, provides further evidence of impaired lipid and fatty acid metabolism (Figure 4c and S4c).

Differently shaped and narrowed cisternae of the ER were observed close to mitochondria, and some even enveloped them. However, the formation of parallel-oriented cisternae of the rough ER, contributing to the creation of the so-called ergastoplasm, was markedly reduced. Some profiles of the smooth ER were enlarged and rounded, providing evidence of changes in the ER collectively related to stress. Along with the increased appearance of pseudo-myelin figures, these changes were indicative of altered lipid formation (Figure 4c and S4c).

### 3.8 | LC acylcarnitines accumulate at harmful levels

In the metabolomic analysis, many LC acylcarnitine species were among the metabolites with the greatest increase in abundance; therefore, the levels of various acylcarnitine species were measured. In the livers of female and male *Hmgcr*-KO mice, the levels of various short- and medium-chain acylcarnitines were unchanged (Figure 4e,f), whereas LC acylcarnitine levels in the liver were increased by 8-fold and 3.5-fold, respectively (Figure 4g,h). A high level of LC acylcarnitine is an indicator of impaired mitochondrial FAO (Dambrova et al., 2022). In addition, increased concentrations of LC acylcarnitine damage mitochondria. In floxed mice liver, LC 3-hydroxy-acylcarnitines were not detected, in contrast to the levels in the *Hmgcr*-KO mice, where the contents of C14, C16 and C18 3-hydroxy-acylcarnitines were substantially elevated (Figure 4i). Accordingly, the increase in 3-hydroxy-acylcarnitine content in *Hmgcr*-KO mouse liver confirms that disrupted mitochondrial fatty acid  $\beta$ -oxidation is the main functional change in *Hmgcr*-KO mouse mitochondria and the reason for the subsequent accumulation of LC acylcarnitines to extremely high levels. The levels of LC acylcarnitines and 3-hydroxy-acylcarnitines were increased several fold, similar to their concentrations in mitochondrial FAOD patients, who present with severe heart, muscle and liver disease symptoms because of deficiencies in LC 3-hydroxy acyl-CoA

dehydrogenase (LCHAD) and mitochondrial trifunctional protein (MTP) (Gillingham et al., 2005; Spiekerkoetter et al., 2009). In *Hmgcr*-KO mice, the accumulation of LC acylcarnitines led to the rapid progression of mitochondrial and cellular damage.

In female and male *Hmgcr*-KO mouse liver, glutamate metabolism also was altered, as indicated by substantially increased glutamate levels in the liver, by as much as fourfold (Figure 4j). ALT converts alanine and glutamate into  $\alpha$ -ketoglutarate, which is a substrate in the citric acid cycle in mitochondria (Lenartowicz & Wojtczak, 1988). According to the respiration measurements taken in the mitochondria of *Hmgcr*-KO mouse liver, the rate of  $\alpha$ -ketoglutarate synthesis from glutamate was probably low. In an alternative pathway, pyruvate is synthesized from amino acids and is a source of gluconeogenesis. In *Hmgcr*-KO mouse liver, a lower level of alanine was in line with an increased level of glutamate, suggesting that the reaction was shifted towards pyruvate and glutamate synthesis and away from  $\alpha$ -ketoglutarate synthesis from alanine. However, even stimulated pyruvate synthesis and gluconeogenesis did not compensate for carbohydrate deficiency.

### 3.9 | Peroxisomal dysfunction

Transcriptomic analysis of *Hmgcr*-KO mouse livers revealed a substantial decrease in the expression of PGC1 $\alpha$ /PPAR $\alpha$  target genes, most of which are crucial for peroxisome formation and function (Figure 5a). Compared with the expression of mitochondrial genes, which was reduced by twofold to threefold, the expression of peroxisomal genes was down-regulated by as much as 30-fold (Figure S3e). A significant decrease was observed in the expression of *Pex* genes, which are required for peroxisome formation (Okumoto et al., 2020). Furthermore, the expression of peroxisomal PPAR $\alpha$  target genes involved in fatty acid transport and metabolism was decreased significantly more than that of PPAR $\alpha$  target genes in mitochondria (Figures 4a and 5a). In fact, the expression of peroxisomal  $\alpha$  and  $\beta$  FAO-related genes was significantly down-regulated by as much as 15-fold compared with the expression in floxed mice liver (Figures 5a and S3e). Moreover, the expression of genes involved in the peroxisome-specific autophagy (pexophagy) pathway, such as **sequestosome 1** (p62/SQSTM1), was significantly up-regulated. p62 is a receptor that promotes peroxisome clustering and enhances pexophagy (Germain & Kim, 2020). In the male *Hmgcr*-KO mice, the expression of the same peroxisomal genes was less affected than that in the female *Hmgcr*-KO mice. The specific effect of PPAR $\alpha$  inactivation in the presence of high fatty acid levels in the liver was explained by the inhibitory effect induced by increased levels of certain fatty acid intermediates. In a past study, indirect evidence suggested that in the presence of LC acylcarnitines, the PPAR $\alpha$  response might be blunted (Chegary et al., 2008). In *Hmgcr*-KO mice, highly abundant LC acylcarnitines might be the intermediates that inhibit PPAR $\alpha$  activity. In the present study, we found that incubation of liver slices in the presence of palmitoylcarnitine markedly reduced PPAR $\alpha$  target gene expression, specifically peroxisome enzyme ACOX1 expression (Figure 5b).

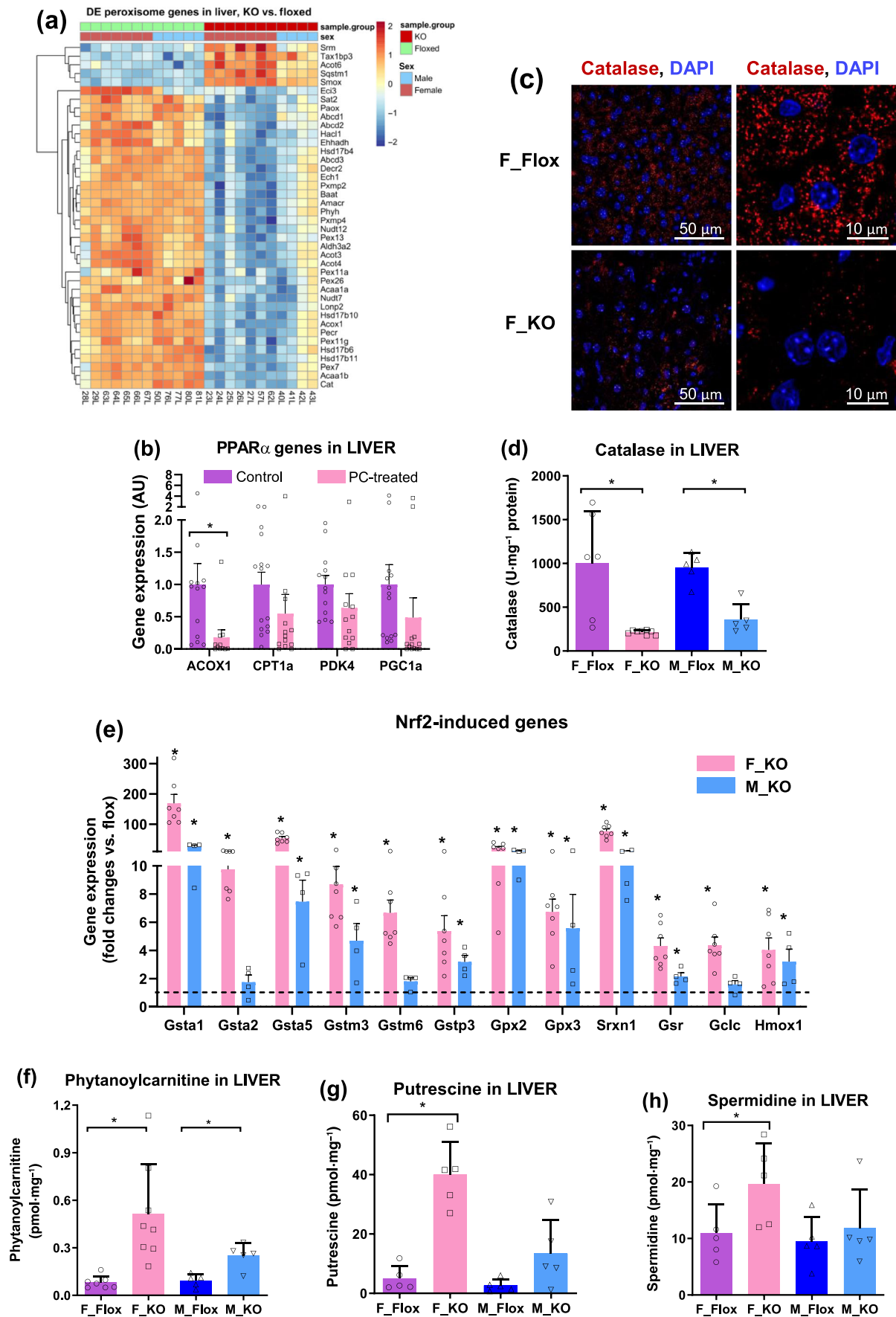


FIGURE 5 Legend on next page.

Catalase is the most abundant protein within peroxisomes. IHC staining of catalase revealed a large loss of peroxisomes in female *Hmgcr*-KO mice (Figure 5c). In addition to lower catalase expression, decreased catalase activity was observed in both female and male *Hmgcr*-KO mice. Catalase activity in the liver tissues of *Hmgcr*-KO mice was reduced by 2.5-fold to 3-fold (Figure 5d). This reduction was comparable with the decrease observed in catalase gene expression. In addition to the disappearance of peroxisomes and reduced catalase activity, activation of the Nrf2 pathway suggested the presence of oxidative damage in the *Hmgcr*-KO mouse liver (Tonelli et al., 2018). We observed marked (up to 50-fold) up-regulation of the expression of Nrf2 pathway genes, including glutathione S-transferase (isoforms A1, A2, A5, M3, M6 and P3), glutathione peroxidase (isoforms 2 and 3), sulfiredoxin-1, glutathione reductase and haem oxygenase-1 (Figure 5e).

**Phytanic acid** is a branched-chain fatty acid that cannot undergo direct  $\beta$ -oxidation because it must first undergo  $\alpha$ -oxidation in peroxisomes. We measured the content of phytanoylcarnitine, which is a marker of peroxisomal dysfunction, in the liver of the *Hmgcr*-KO mice (Herzog et al., 2017). In female *Hmgcr*-KO mice, the content of phytanoylcarnitine in the liver was sixfold increased, while in males, an increase of approximately threefold was observed (Figure 5f), suggesting a substantially decreased peroxisomal  $\alpha$ -oxidation rate. In addition, peroxisomal polyamine metabolism was disrupted, resulting in a significant increase in the levels of **putrescine** and **spermidine** in female *Hmgcr*-KO mouse liver (Figure 5g,h). On Day 5, the number of peroxisomes, the catalase activity level and the phytanoylcarnitine level in *Hmgcr*-KO mouse liver were similar to those observed in control mice; these results indicated that peroxisome damage was secondary to mitochondrial dysfunction.

### 3.10 | ER stress

In previous studies, ER stress has been suggested to be the main cause of intracellular dysfunction in *Hmgcr*-KO mice; therefore, ER stress-induced gene expression and changes in the abundance of several ER-generated metabolites were evaluated. Indeed, the mRNA levels of the canonical ER stress genes *Atf4*, *Atf6*, *Ddit3* and *Trib3* showed a significant 2-fold to 19-fold increase (Figure 6a).

To estimate changes in ER functionality, the content of metabolites synthesized in the ER was evaluated. For example, the de novo ceramide biosynthesis pathway is activated in the ER when lipid homeostasis is disrupted (Kim & Bai, 2022; McNally et al., 2022). Therefore, we measured the ceramide levels and found increased levels of ceramides and their synthesis precursors, dihydroceramides, which have been previously associated with ER stress (McNally et al., 2022). In the female and male *Hmgcr*-KO mouse livers, the dihydroceramide levels were increased by approximately 2.5-fold, while the ceramide levels were increased by 60%, indicating activation of the ceramide synthesis pathway (Figure 6b,c). In addition, we observed a slight decrease in the level of sphingomyelin, which can be converted into ceramide via the salvage pathway in lysosomes or the sphingomyelinase pathway in the plasma membrane, Golgi and mitochondria (Figure 6d). These data indicate that ER stress can promote the activation of the ceramide synthesis pathway.

The ER is the major site for the synthesis of diglycerides and triglycerides. In female and male *Hmgcr*-KO mice, we found that the triglyceride contents in the liver were increased by 7-fold to 19-fold, causing severe steatosis, while lower triglyceride concentrations were present in plasma (Figure 2g,h). These results indicated that triglyceride synthesis in the ER was not affected in *Hmgcr*-KO mice. Notably, dysregulation of intrahepatic lipid metabolism in mitochondria led to steatosis in the *Hmgcr*-KO mouse liver.

Bile acids are primarily synthesized from cholesterol in the liver by enzymes located mainly in the ER, with some also present in peroxisomes, mitochondria and the cytosol (Russell, 2003). The **cholic acid** content in the female KO mouse liver was reduced, but the difference was not statistically significant due to variabilities in the female floxed group (Figure 6e). The reduced cholic acid content may have been caused by the reduced availability of cholesterol and down-regulated de novo bile acid synthesis pathways in *Hmgcr*-KO mice. Transcriptional analysis revealed that bile biosynthesis might be inhibited because the gene expression of enzymes involved in the classical bile acid synthesis pathway (*CYP7A1*, *CYP8B1* and *HSD3B7*) and alternative pathway (*CYP27A1*, peroxisomal and mitochondrial  $\beta$ -oxidation enzymes) was down-regulated by as much as 40-fold. Plasma concentrations of cholic acid were similar in floxed and *Hmgcr*-KO animals (Figure 6f). In contrast, the concentrations of conjugated bile acids, including **taurocholic acid** and **glycocholic acid**, were substantially

**FIGURE 5** *Hmgcr*-knockout (KO) mice livers are lacking peroxisomes and their functionality. (a) In the *Hmgcr*-KO mice liver, genes related to peroxisomal formation and fatty acid metabolism are significantly down-regulated. (b) Incubation of control mice liver slices with palmitoylcarnitine (PC) reduced peroxisome proliferator-activated receptor alpha (PPAR $\alpha$ ) target gene expression. (c) Very few catalase-positive peroxisomes were detected in the liver slices of KO mice. (d) A similar decrease was observed in catalase activity. (e) Excessive activation of genes from the Nrf2 pathway indicates oxidative stress in the livers of KO mice. (f) The increased content of phytanoylcarnitine suggests markedly decreased peroxisomal  $\alpha$ -oxidation. (g, h) Putrescine and spermidine levels were significantly increased in the KO mouse liver because polyamine metabolism is disturbed. Liver tissue samples were collected from floxed and KO male and female mice at the endpoint (Days 7–10). Data are shown as the mean  $\pm$  SEM ( $n = 5$ –8 mice per group). \* $P < 0.05$ , versus the corresponding sex of floxed mice, one-way analysis of variance (ANOVA) followed by unpaired *t*-test post hoc analysis. DAPI, 4',6-diamidino-2-phenylindole, a nuclear staining dye; F\_Floxed, floxed female; F\_KO, knockout female; *Gclc*, glutamate-cysteine ligase catalytic subunit; *Gpx2* and *Gpx3*, glutathione peroxidase 2 and 3; *Gsr*, glutathione reductase; *Gsta1*, *Gsta2* and *Gsta5*, glutathione S-transferase alpha 1, 2 and 5; *Gstm3* and *Gstm6*, glutathione S-transferase Mu3 and Mu6; *Gstp3*, glutathione S-transferase Pi3; *Hmox1*, haem oxygenase 1; M\_Floxed, floxed male; M\_KO, knockout male; *Nrf2*, nuclear factor erythroid 2-related factor 2; *Srxn1*, sulfiredoxin 1.

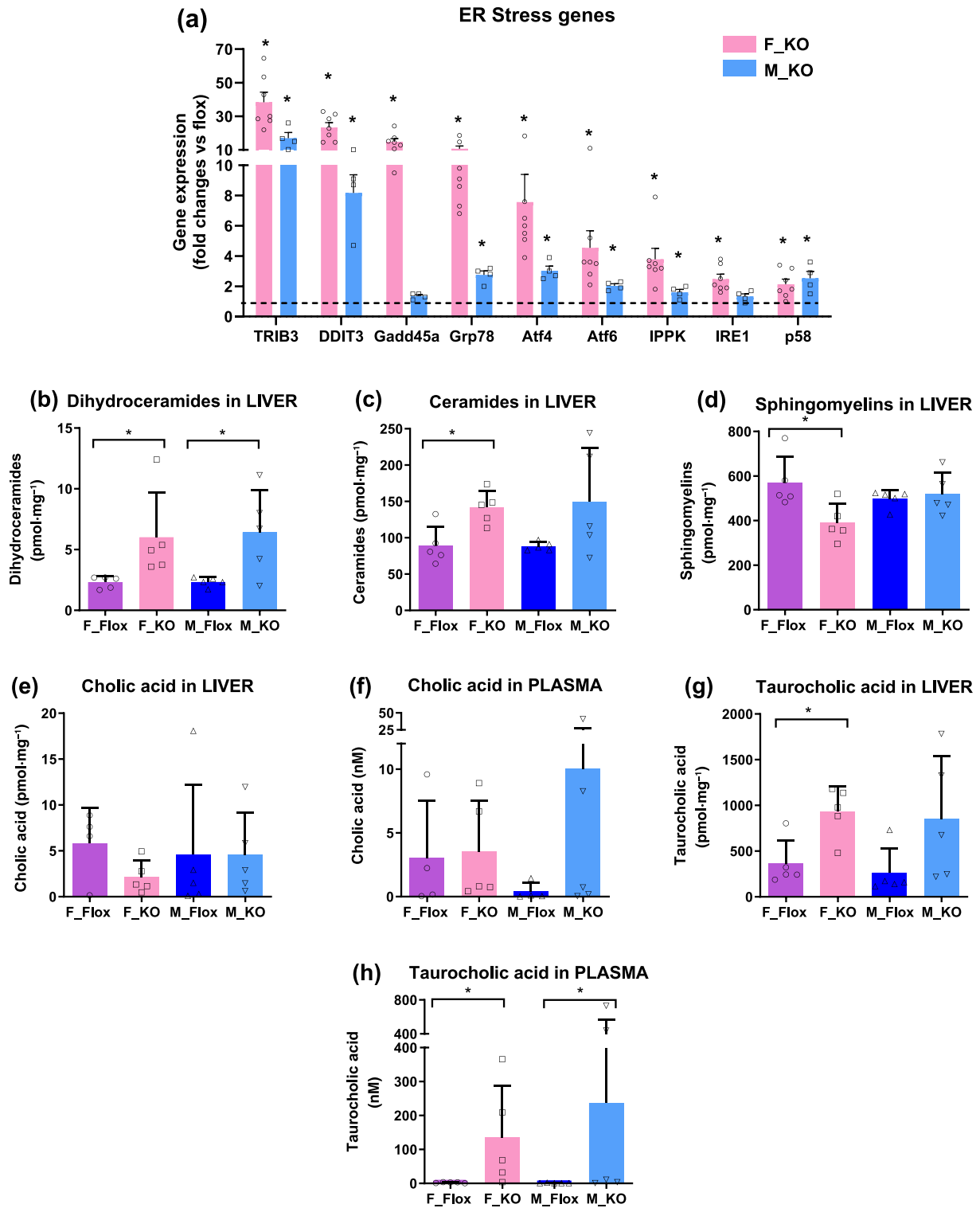


**FIGURE 6** Legend on next page.

increased in the liver and plasma of the *Hmgcr*-KO animals (Figure 6g,h). In line with the histological findings, cholestasis may be a reason for disrupted bile acid turnover. Overall, ER stress in *Hmgcr*-KO animals might be a secondary effect of fatty acid metabolism disruptions in mitochondria and peroxisomes.

## 4 | DISCUSSION

We have elucidated the pathways related to the detrimental effects observed in *Hmgcr*-KO mice, to understand the mechanism underlying the negative phenotype acquired by patients taking statins. The link between alterations in HMGR expression and mitochondrial and peroxisomal function has not been previously studied in detail. Here, we show that HMGR is essential for the mitochondrial  $\beta$ -oxidation pathway of fatty acids. The loss of HMGR was characterized by a very high accumulation of LC acylcarnitines and LC fatty acids at levels known to cause cell death. These metabolic changes induced rapidly progressing liver damage, leading to death without apparently damaging other tissues.

The time-dependent analysis of the development of fatal liver failure, within Days 5–11, revealed that the primary effect of *Hmgcr* gene KO was a reduction in the mitochondrial FAO rate. Any other metabolic functions, including peroxisomal and ER functionality, at an earlier time point (Day 5) were not affected by *Hmgcr*-KO. This outcome suggests that initial detrimental changes in mitochondrial fatty acid metabolism were compensated by the oxidation of other substrates that maintained ATP production in the liver, to prevent energy deficiency and maintain overall liver functionality. We found a slight increase in plasma ALT concentration in female *Hmgcr*-KO mice on Day 5, suggesting that some cells had been disrupted at this time point. Furthermore, reduced mitochondrial FAO resulted in the accumulation of LC fatty acids, triglycerides and LC acylcarnitines, which are the most harmful of metabolism intermediates. Our observations are in line with a previous study that demonstrated lethal outcomes within 6 weeks of age due to disturbances in lipid metabolism (shift to lipogenesis and accumulation) and hypoglycaemia in liver-specific *Hmgcr*-KO mice (Nagashima et al., 2012). Detrimental changes in metabolism rapidly induce a severe phenotype when a certain limit of *Hmgcr* gene expression is reached; however, some animals can survive and recover if tissues can overcome the metabolic crisis (De Giorgi et al., 2020; Nagashima et al., 2012). This

might be an important aspect for the recovery from statin-induced adverse reactions.

Previous studies have shown that LC acylcarnitines are abundant in mitochondria, can inhibit pyruvate and lactate metabolism and, at higher concentrations, inhibit ATP synthesis. Therefore, they are very harmful fatty acid intermediates (Liepinsh et al., 2016; McCoin et al., 2015; Tominaga et al., 2008). In female *Hmgcr*-KO mouse livers, the LC acylcarnitine levels were increased by as much as 12-fold, which was comparable with levels found in patients with lethal inherited FAOD (Begrache et al., 2011; Di Pasqua et al., 2022; North et al., 1995; Pessayre et al., 2012; Wanders et al., 2020). Depending on which enzyme or transporter level is deficient, the levels of LC acylcarnitines in plasma can be elevated by several fold. A comparable increase in LC acylcarnitines has been measured in skin fibroblasts isolated from FAOD patients (Okun et al., 2002; Ventura et al., 1999). A distinct feature of *Hmgcr*-KO mice in our study was increased levels of hydroxyacylcarnitines that are unique to mitochondrial FAOD patients deficient in LCHAD, which is an enzyme of MTP. In comparison with other enzyme deficiencies in FAOD patients, LCHAD (TFP) deficiency along with cardiomyopathy and liver damage develops long-term irreversible neuropathic complications, most likely due to the accumulation of toxic concentrations (as high as 16  $\mu$ M) of LC 3-hydroxy-acylcarnitines in patient plasma (Gillingham et al., 2005; Spiekerkoetter et al., 2009). Overall, mitochondrial damage, energy deficiency and liver cell death were caused by LC acylcarnitine accumulation and may be attributable to inhibited LCHAD activity in *Hmgcr*-KO mouse livers (Figure 7).

Peroxisome biogenesis and degradation are very rapid processes leading to a peroxisome half-life of 1.5–2 days (Kim & Bai, 2022). Transcriptomic analysis of *Hmgcr*-KO mice revealed a significant reduction in the expression of PGC1 $\alpha$ /PPAR $\alpha$  target genes that are important for peroxisomal formation and function. Through IHC analysis, we found a lower number of peroxisomes, which might have been due to insufficient formation and accelerated pexophagy. Notably, LC fatty acids were metabolized to short- and medium-chain fatty acids by peroxisomal  $\beta$ -oxidation. Hence, peroxisomes can partially compensate for lower FAO rates in mitochondria (Houten et al., 2020) to prevent the accumulation of LC fatty acids and their metabolic intermediates (Liepinsh et al., 2013). In *Hmgcr*-KO mice, acylcarnitine-induced lipotoxicity at the endpoint indicated that peroxisomes in these mice were not formed and could not compensate for mitochondrial dysfunction. Moreover, the absence of peroxisomal fatty acid

**FIGURE 6** In the *Hmgcr*-knockout (KO) mice livers, endoplasmic reticulum (ER) stress-related gene expression was increased, but ER lipid metabolism functions were fully maintained. (a) The levels of canonical ER stress genes showed a significant increase in the *Hmgcr*-KO mice livers. (b) Dihydroceramide and (c) ceramide levels were increased, indicating an activated ceramide synthesis pathway. (d) The decreased content of sphingomyelins can be the result of their conversion into ceramides. (e, f) De novo synthesis of cholic acid is not changed, (g, h) while cholestasis induces increased levels of conjugated bile acids in KO mice livers. Liver tissue and plasma samples were collected from floxed and KO male and female mice at the endpoint (Days 7–10). Data are shown as the mean  $\pm$  SEM ( $n = 5$ –8 mice per group). \* $P < 0.05$ , versus the corresponding sex of floxed mice, one-way analysis of variance (ANOVA) followed by unpaired  $t$ -test post hoc analysis. *Atf4* and *Atf6*, activating transcription factors 4 and 6; *Ddit3*, DNA damage-inducible transcript 3; F\_Flox, floxed female; F\_KO, knockout female; *Gadd45a*, growth arrest and DNA damage-inducible alpha; *Grp78*, glucose-regulated protein; *lppk*, inositol-pentakisphosphate 2-kinase; *lre1*, inositol-requiring enzyme 1; M\_Flox, floxed male; M\_KO, knockout male; *Trib3*, tribbles homologue 3.

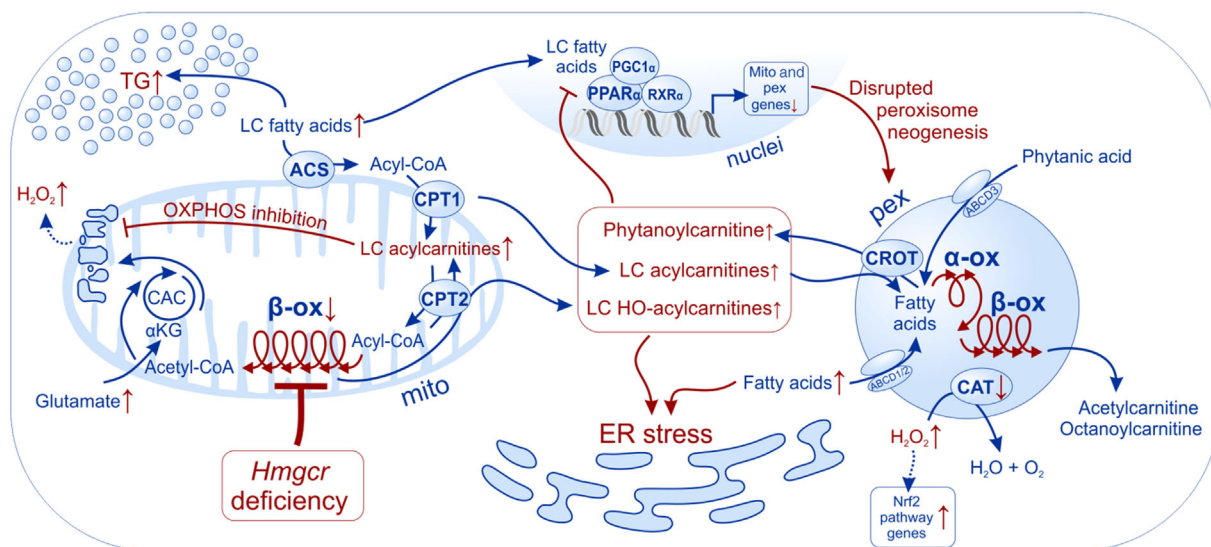


**FIGURE 7** Energy metabolism changes in *Hmgcr*-knockout (KO) mice. The primary effect in the liver of the KO mouse is a reduced mitochondrial FAO rate (see Figure 4) that leads to the accumulation of long-chain acylcarnitines and 3-hydroxy-acylcarnitines (see Figure 4). In mitochondria, long-chain acylcarnitines inhibit oxidative phosphorylation that results in increased reactive oxygen species (ROS) production (Liepinsh et al., 2016; Tominaga et al., 2008). Long-chain acylcarnitines leak from mitochondria and can be metabolized in peroxisomes (Houten et al., 2020; Liepinsh et al., 2013), thus compensating for reduced mitochondrial function. Further accumulation of lipid intermediates disrupts peroxisome neogenesis by suppressing peroxisome proliferator-activated receptor alpha (PPAR $\alpha$ )/PPAR gamma coactivator-1 alpha (PGC1 $\alpha$ ) activity (see Figure 5) that leads to increased levels of branched-chain acylcarnitines (e.g., phytanoylcarnitine) (see Figure 5) and H<sub>2</sub>O<sub>2</sub>, which further activate the nuclear factor erythroid 2-related factor 2 (Nrf2) pathway (see Figure 5). Disruptions of peroxisomes accelerate the progression of cell damage. Increased levels of long-chain fatty acids, acylcarnitines and ROS induce endoplasmic reticulum (ER) stress (see Figure 6). ABCD1/2 and ABCD3, ATP-binding cassette subfamily D members 1/2 and 3; ACS, acyl-CoA synthetase; CAC, citric acid cycle; CAT, catalase; CPT1 and CPT2, carnitine palmitoyltransferase 1 and 2; CROT, carnitine *O*-octanoyltransferase; LC fatty acids, long-chain fatty acids; LC, long-chain; mito, mitochondria; OXPHOS, oxidative phosphorylation; pex, peroxisome; RXR $\alpha$ , retinoid X receptor alpha; TG, triglycerides;  $\alpha$ KG,  $\alpha$ -ketoglutarate;  $\alpha$ -ox,  $\alpha$ -oxidation;  $\beta$ -ox,  $\beta$ -oxidation.

metabolism led to the accumulation of a peroxisome-specific substrate, phytanoylcarnitine. Hence, we hypothesize that increased levels of LC acylcarnitines might damage peroxisomes as well as decrease PPAR $\alpha$  activity. Peroxisomes generate approximately 35% of H<sub>2</sub>O<sub>2</sub> in cells, and therefore, most catalase in a cell is located in peroxisomes (Kim & Bai, 2022). In the *Hmgcr*-KO mouse liver, disruption to peroxisome function leads to a lower antioxidant capacity and higher oxidative damage in liver cells. Overall, because peroxisomes play an important role in cell function, liver failure rapidly progresses and becomes irreversible when peroxisomal metabolic and catalase functions are disrupted.

Previous studies of tissue-specific *Hmgcr*-KO mice emphasized ER stress as the central pathological mechanism (De Giorgi et al., 2020). Because the ER is a major site of protein synthesis and folding, lipid and steroid synthesis, carbohydrate metabolism and calcium storage, prolonged ER stress might disrupt lipid metabolism and induce hepatic lipotoxicity (Zhang et al., 2021). In this study, the ER stress response and changes in corresponding lipid levels were observed only at the endpoint. The ER contacts mitochondria and peroxisomes through multiple sites, and these sites advance the communication and transfer of metabolites between organelles, ensuring the regulation of lipid homeostasis and other biological functions such as apoptosis (Kim & Bai, 2022; Zhang et al., 2021). Therefore, mitochondrial metabolic stress as well as peroxisome deficiency can trigger an

ER stress response (Kovacs et al., 2012; Su et al., 2014). In addition, elevated levels of LC acylcarnitines can be part of lipid overload-induced ER stress. Considering the time-dependent effects in mitochondria, peroxisomes and ER observed in this study, ER stress in the *Hmgcr*-KO mouse liver is a late response that is induced after mitochondrial and peroxisomal functionality is compromised.

Despite their beneficial effects related to a decrease in high cholesterol levels, statins also produce adverse reactions primarily in the liver and skeletal muscles (Newman et al., 2019), while the mechanisms of statin intolerance are still under investigation. Previous studies of tissue-specific *Hmgcr*-KO demonstrated that enzyme function is a crucial requirement for cell survival, independent of cell and tissue type (De Giorgi et al., 2020; Lacher et al., 2017; Osaki et al., 2015; Takei et al., 2020; Yeh et al., 2018). Our study provides evidence that *Hmgcr* enzyme deficiency in the liver leads to mitochondrial and peroxisomal dysfunction that is initiated by impaired FAO. These findings are in line with studies showing that mitochondrial dysfunction and the manifestation of abnormal lipid metabolism are important hallmarks of statin-associated skeletal muscle damage (Mollazadeh et al., 2021). The severity of statin-induced effects on mitochondrial functionality depends on statin bioavailability in the respective tissue (Christiansen et al., 2021) and a combination of factors such as genetics, age and polypharmacy.

Statin-induced myopathy is more frequent in patients with CPT2 mutations (Vladutiu et al., 2006). The CPT2 mutation can cause mitochondrial FAOD and the accumulation of LC acylcarnitines (McCormick & Chirila, 2021). Fasting and exercise are thought to accelerate statin-induced tissue injury (Deichmann et al., 2015; Parker et al., 2012), and both fasting and exercise can cause an increase in LC acylcarnitine levels (Dambrova et al., 2022). Statin treatment may lower the respiratory capacity of mitochondrial complexes and fatty acid  $\beta$ -oxidation via inhibited HMGCR activity and can therefore result in a direct increase of LC acylcarnitine levels in tissues. Female *Hmgcr*-KO animals showed marked mitochondrial dysfunction, including altered FAO at an early time point, followed by a marked accumulation of acylcarnitines at the endpoint, suggesting detrimental events and consequences similar to those induced by statins. Thus, mitochondrial  $\beta$ -oxidation dysfunction, which contributes to elevated levels of LC acylcarnitines, may be an important mechanism determining the progression and severity of statin-induced tissue damage.

In conclusion, the livers of *Hmgcr*-KO mice showed rapid disruption of mitochondrial fatty acid  $\beta$ -oxidation, leading to the harmful accumulation of LC acylcarnitines. Further progression of liver failure was induced by abrogated mitochondrial and peroxisomal fatty acid metabolism, enhanced glucose utilization in the liver and whole-body hypoglycaemia. HMGCR activity is thus mandatory for mitochondrial functionality to maintain energy metabolism balance; accordingly, statin-induced adverse reactions might be rescued by the prevention of acylcarnitine accumulation. This study suggests that further research on LC acylcarnitine accumulation in patients taking statins should be performed.

#### AUTHOR CONTRIBUTIONS

**Edgars Liepinsh:** Conceptualization (equal); data curation (equal); formal analysis (equal); investigation (equal); visualization (equal); writing—original draft (equal); writing—review and editing (equal). **Liga Zvejniece:** Conceptualization (equal); formal analysis (equal); investigation (equal); writing—original draft (equal); writing—review and editing (equal). **Laura Clemensson:** Conceptualization (equal); formal analysis (equal); writing—review and editing (equal). **Melita Ozola:** Formal analysis (equal); writing—original draft (equal); writing—review and editing (equal). **Edijs Vavars:** Formal analysis (equal); investigation (equal); writing—original draft (supporting); writing—review and editing (equal). **Helena Cirule:** Investigation (equal); writing—review and editing (supporting). **Stanislava Korzh:** Formal analysis (equal); investigation (equal); writing—review and editing (supporting). **Sandra Skuja:** Formal analysis (equal); investigation (equal); writing—review and editing (equal). **Valerija Groma:** Formal analysis (equal); investigation (equal); writing—review and editing (equal). **Monta Briviba:** Formal analysis (equal); investigation (equal); writing—review and editing (supporting). **Solveiga Grinberga:** Formal analysis (equal); investigation (equal); writing—original draft (supporting); writing—review and editing (supporting). **Wen Liu:** Formal analysis (equal). **Paweł Olszewski:** Formal analysis (equal); writing—original draft (supporting); writing—review and editing (equal). **Mélissa Gentreau:** Formal analysis (equal); writing—original draft (supporting); writing—review and editing (equal).

**Robert Fredriksson:** Formal analysis (equal); writing—review and editing (supporting). **Maija Dambrova:** Conceptualization (equal); writing—original draft (equal); writing—review and editing (equal). **Helgi Schiöth:** Conceptualization (equal); writing—original draft (equal); writing—review and editing (equal).

#### ACKNOWLEDGEMENTS

HBS is supported by the Swedish Research Council (Vetenskapsrådet [2019-01066 and 2022-00562]) and the Novo Nordisk Foundation (Novo Nordisk Fonden). MD and HC were supported by the Latvian Council of Science (Latvijas Zinātnes Padome [Grant No. LZP-2023/1-0287]). The authors were supported by the European Union's Horizon 2020 Framework Programme, Project FAT4BRAIN (Grant No. 857394). The authors acknowledge the access to the infrastructure and expertise of the Baltic Biomaterials Centre of Excellence (BBCE) (European Union's Horizon 2020 Framework Programme under Grant Agreement No. 857287).

#### CONFLICT OF INTEREST STATEMENT

The authors declare no conflicts of interest.

#### DATA AVAILABILITY STATEMENT

The data are submitted as [supporting information](#).

#### DECLARATION OF TRANSPARENCY AND SCIENTIFIC RIGOUR

This Declaration acknowledges that this paper adheres to the principles for transparent reporting and scientific rigour of preclinical research as stated in the *BJP* guidelines for [Design & Analysis](#), [Immunoblotting and Immunochemistry](#), and [Animal Experimentation](#) and as recommended by funding agencies, publishers and other organizations engaged with supporting research.

#### ORCID

**Edgars Liepinsh**  <https://orcid.org/0000-0003-2213-8337>

**Liga Zvejniece**  <https://orcid.org/0000-0003-4576-2386>

#### REFERENCES

- Ahmad, T., Kelly, J. P., McGarrah, R. W., Hellkamp, A. S., Fiuzat, M., Testani, J. M., Wang, T. S., Verma, A., Samsky, M. D., Donahue, M. P., Ilkayeva, O. R., Bowles, D. E., Patel, C. B., Milano, C. A., Rogers, J. G., Felker, G. M., O'Connor, C. M., Shah, S. H., & Kraus, W. E. (2016). Prognostic implications of long-chain acylcarnitines in heart failure and reversibility with mechanical circulatory support. *Journal of the American College of Cardiology*, 67(3), 291–299. <https://doi.org/10.1016/j.jacc.2015.10.079>
- Alexander, S. P., Fabbro, D., Kelly, E., Mathie, A., Peters, J. A., Veale, E. L., Armstrong, J. F., Faccenda, E., Harding, S. D., Pawson, A. J., Southan, C., Davies, J. A., Annett, S., Boison, D., Burns, K. E., Dessauer, C., Gertsch, J., Helsby, N. A., Izzo, A. A., ... Wong, S. S. (2021). The Concise Guide to PHARMACOLOGY 2021/22: Enzymes. *British Journal of Pharmacology*, 178(Suppl 1), S313–S411. <https://doi.org/10.1111/bph.15542>
- Alexander, S. P., Kelly, E., Marrion, N. V., Peters, J. A., Faccenda, E., Harding, S. D., Pawson, A. J., Sharman, J. L., Southan, C., Buneman, O. P., Cidrowski, J. A., Christopoulos, A., Davenport, A. P., Fabbro, D.,

- Spedding, M., Striessnig, J., & Davies, J. A. (2017). The Concise Guide to PHARMACOLOGY 2017/18: Overview. *British Journal of Pharmacology*, 174, S1–S16. <https://doi.org/10.1111/bph.13882>
- Begrache, K., Massart, J., Robin, M. A., Borgne-Sanchez, A., & Fromenty, B. (2011). Drug-induced toxicity on mitochondria and lipid metabolism: Mechanistic diversity and deleterious consequences for the liver. *Journal of Hepatology*, 54(4), 773–794. <https://doi.org/10.1016/j.jhep.2010.11.006>
- Besse-Patin, A., Jeromson, S., Levesque-Damphousse, P., Secco, B., Laplante, M., & Estall, J. L. (2019). PGC1A regulates the IRS1:IRS2 ratio during fasting to influence hepatic metabolism downstream of insulin. *Proceedings of the National Academy of Sciences of the United States of America*, 116(10), 4285–4290. <https://doi.org/10.1073/pnas.1815150116>
- Bhuiyan, J., & Seccombe, D. W. (1996). The effects of 3-hydroxy-3-methylglutaryl-CoA reductase inhibition on tissue levels of carnitine and carnitine acyltransferase activity in the rabbit. *Lipids*, 31(8), 867–870. <https://doi.org/10.1007/BF02522982>
- Chambers, K. T., Chen, Z., Lai, L., Leone, T. C., Towle, H. C., Kralli, A., Crawford, P. A., & Finck, B. N. (2013). PGC-1 $\beta$  and ChREBP partner to cooperatively regulate hepatic lipogenesis in a glucose concentration-dependent manner. *Molecular Metabolism*, 2(3), 194–204. <https://doi.org/10.1016/j.molmet.2013.05.001>
- Chegary, M., Te Brinke, H., Doolaard, M., IJlst, L., Wijburg, F. A., Wanders, R. J., & Houten, S. M. (2008). Characterization of L-aminocarnitine, an inhibitor of fatty acid oxidation. *Molecular Genetics and Metabolism*, 93(4), 403–410. <https://doi.org/10.1016/j.ymgme.2007.11.001>
- Chen, S., Zhou, Y., Chen, Y., & Gu, J. (2018). fastp: An ultra-fast all-in-one FASTQ preprocessor. *Bioinformatics*, 34(17), i884–i890. <https://doi.org/10.1093/bioinformatics/bty560>
- Christiansen, L. B., Dohmann, T. L., Ludvigsen, T. P., Parfieniuk, E., Ciborowski, M., Szczerbinski, L., Kretowski, A., Desler, C., Tiano, L., Orlando, P., Martinussen, T., Olsen, L. H., & Larsen, S. (2021). Atorvastatin impairs liver mitochondrial function in obese Gottingen Minipigs but heart and skeletal muscle are not affected. *Scientific Reports*, 11(1), 2167. <https://doi.org/10.1038/s41598-021-81846-9>
- Colantonio, L. D., Rosenson, R. S., Deng, L., Monda, K. L., Dai, Y., Farkouh, M. E., Safford, M. M., Philip, K., Mues, K. E., & Muntner, P. (2019). Adherence to statin therapy among US adults between 2007 and 2014. *Journal of the American Heart Association*, 8(1), e010376. <https://doi.org/10.1161/JAHA.118.010376>
- Curtis, M. J., Alexander, S. P. H., Cirino, G., George, C. H., Kendall, D. A., Insel, P. A., Izzo, A. A., Ji, Y., Panettieri, R. A., Patel, H. H., Sobey, C. G., Stanford, S. C., Stanley, P., Stefanska, B., Stephens, G. J., Teixeira, M. M., Vergnolle, N., & Ahluwalia, A. (2022). Planning experiments: Updated guidance on experimental design and analysis and their reporting III. *British Journal of Pharmacology*, 179, 3907–3913. <https://doi.org/10.1111/bph.15868>
- Dambrova, M., Makrecka-Kuka, M., Kuka, J., Vilskersts, R., Nordberg, D., Attwood, M. M., Smesny, S., Sen, Z. D., Guo, A. C., Oler, E., Tian, S., Zheng, J., Wishart, D. S., Liepinsh, E., & Schiöth, H. B. (2022). Acylcarnitines: Nomenclature, biomarkers, therapeutic potential, drug targets, and clinical trials. *Pharmacological Reviews*, 74(3), 506–551. <https://doi.org/10.1124/pharmrev.121.000408>
- de Giorgi, M., Jarrett, K. E., Burton, J. C., Doerfler, A. M., Hurley, A., Li, A., Hsu, R. H., Furgurson, M., Patel, K. R., Han, J., Borchers, C. H., & Lagor, W. R. (2020). Depletion of essential isoprenoids and ER stress induction following acute liver-specific deletion of HMG-CoA reductase. *Journal of Lipid Research*, 61(12), 1675–1686. <https://doi.org/10.1194/jlr.RA120001006>
- Deichmann, R. E., Lavie, C. J., Asher, T., DiNicolantonio, J. J., O'Keefe, J. H., & Thompson, P. D. (2015). The interaction between statins and exercise: Mechanisms and strategies to counter the musculo-skeletal side effects of this combination therapy. *The Ochsner Journal*, 15(4), 429–437.
- Di Cara, F., Savary, S., Kovacs, W. J., Kim, P., & Rachubinski, R. A. (2023). The peroxisome: An up-and-coming organelle in immunometabolism. *Trends in Cell Biology*, 33(1), 70–86. <https://doi.org/10.1016/j.tcb.2022.06.001>
- Di Pasqua, L. G., Cagna, M., Berardo, C., Vairetti, M., & Ferrigno, A. (2022). Detailed molecular mechanisms involved in drug-induced non-alcoholic fatty liver disease and non-alcoholic steatohepatitis: An update. *Biomedicine*, 10, 194. <https://doi.org/10.3390/biomedicines10010194>
- Germain, K., & Kim, P. K. (2020). Pexophagy: A model for selective autophagy. *International Journal of Molecular Sciences*, 21, 578. <https://doi.org/10.3390/ijms21020578>
- Gillingham, M. B., Weleber, R. G., Neuringer, M., Connor, W. E., Mills, M., van Calcar, S., ver Hoeve, J., Wolff, J., & Harding, C. O. (2005). Effect of optimal dietary therapy upon visual function in children with long-chain 3-hydroxyacyl CoA dehydrogenase and trifunctional protein deficiency. *Molecular Genetics and Metabolism*, 86(1–2), 124–133. <https://doi.org/10.1016/j.ymgme.2005.06.001>
- Goldstein, J. L., & Brown, M. S. (2015). A century of cholesterol and coronaries: From plaques to genes to statins. *Cell*, 161(1), 161–172. <https://doi.org/10.1016/j.cell.2015.01.036>
- Herzog, K., van Lenthe, H., Wanders, R. J. A., Vaz, F. M., Waterham, H. R., & Ferdinandusse, S. (2017). Identification and diagnostic value of phytanoyl- and pristanoyl-carnitine in plasma from patients with peroxisomal disorders. *Molecular Genetics and Metabolism*, 121(3), 279–282. <https://doi.org/10.1016/j.ymgme.2017.05.003>
- Houten, S. M., Wanders, R. J. A., & Ranea-Robles, P. (2020). Metabolic interactions between peroxisomes and mitochondria with a special focus on acylcarnitine metabolism. *Biochimica et Biophysica Acta—Molecular Basis of Disease*, 1866(5), 165720. <https://doi.org/10.1016/j.bbadis.2020.165720>
- Kim, J., & Bai, H. (2022). Peroxisomal stress response and inter-organelle communication in cellular homeostasis and aging. *Antioxidants (Basel)*, 11, 192. <https://doi.org/10.3390/antiox11020192>
- Knottnerus, S. J. G., Bleeker, J. C., Wüst, R. C. I., Ferdinandusse, S., IJlst, L., Wijburg, F. A., Wanders, R. J. A., Visser, G., & Houtkoper, R. H. (2018). Disorders of mitochondrial long-chain fatty acid oxidation and the carnitine shuttle. *Reviews in Endocrine & Metabolic Disorders*, 19(1), 93–106. <https://doi.org/10.1007/s11154-018-9448-1>
- Kovacs, W. J., Charles, K. N., Walter, K. M., Shackelford, J. E., Wikander, T. M., Richards, M. J., Fliesler, S. J., Krisans, S. K., & Faust, P. L. (2012). Peroxisome deficiency-induced ER stress and SREBP-2 pathway activation in the liver of newborn PEX2 knock-out mice. *Biochimica et Biophysica Acta*, 1821(6), 895–907. <https://doi.org/10.1016/j.bbailip.2012.02.011>
- Lacher, S. M., Bruttger, J., Kalt, B., Berthelet, J., Rajalingam, K., Wortge, S., & Waisman, A. (2017). HMG-CoA reductase promotes protein prenylation and therefore is indispensable for T-cell survival. *Cell Death & Disease*, 8(5), e2824. <https://doi.org/10.1038/cddis.2017.221>
- Lenartowicz, E., & Wojtczak, A. B. (1988). Significance of the alanine aminotransferase reaction in the formation of  $\alpha$ -ketoglutarate in rat liver mitochondria. *Archives of Biochemistry and Biophysics*, 260(1), 309–319. [https://doi.org/10.1016/0003-9861\(88\)90455-9](https://doi.org/10.1016/0003-9861(88)90455-9)
- Liao, Y., Smyth, G. K., & Shi, W. (2019). The R package Rsubread is easier, faster, cheaper and better for alignment and quantification of RNA sequencing reads. *Nucleic Acids Research*, 47(8), e47. <https://doi.org/10.1093/nar/gkz114>
- Liepinsh, E., Makrecka-Kuka, M., Makarova, E., Volska, K., Vilks, K., Sevostjanovs, E., Antone, U., Kuka, J., Vilskersts, R., Lola, D., Loza, E., Grinberga, S., & Dambrova, M. (2017). Acute and long-term administration of palmitoylcarnitine induces muscle-specific insulin resistance in mice. *BioFactors*, 43(5), 718–730. <https://doi.org/10.1002/biof.1378>
- Liepinsh, E., Makrecka-Kuka, M., Volska, K., Kuka, J., Makarova, E., Antone, U., Sevostjanovs, E., Vilskersts, R., Strods, A., Tars, K., &

- Dambrova, M. (2016). Long-chain acylcarnitines determine ischaemia/reperfusion-induced damage in heart mitochondria. *The Biochemical Journal*, 473, 1191–1202. <https://doi.org/10.1042/BCJ20160164>
- Liepinsh, E., Skapare, E., Kuka, J., Makrecka, M., Cirule, H., Vavers, E., Sevostjanovs, E., Grinberga, S., Pugovics, O., & Dambrova, M. (2013). Activated peroxisomal fatty acid metabolism improves cardiac recovery in ischemia-reperfusion. *Naunyn-Schmiedeberg's Archives of Pharmacology*, 386(6), 541–550. <https://doi.org/10.1007/s00210-013-0849-0>
- Lilley, E., Stanford, S. C., Kendall, D. E., Alexander, S. P. H., Cirino, G., Docherty, J. R., George, C. H., Insel, P. A., Izzo, A. A., Ji, Y., Panettieri, R. A., Sobey, C. G., Stefanska, B., Stephens, G., Teixeira, M., & Ahluwalia, A. (2020). ARRIVE 2.0 and the British Journal of Pharmacology: Updated guidance for 2020. *British Journal of Pharmacology*, 177, 3611–3616. <https://doi.org/10.1111/bph.15178>
- Love, M. I., Huber, W., & Anders, S. (2014). Moderated estimation of fold change and dispersion for RNA-seq data with DESeq2. *Genome Biology*, 15(12), 550. <https://doi.org/10.1186/s13059-014-0550-8>
- McCoin, C. S., Knotts, T. A., & Adams, S. H. (2015). Acylcarnitines—Old actors auditioning for new roles in metabolic physiology. *Nature Reviews. Endocrinology*, 11(10), 617–625. <https://doi.org/10.1038/nrendo.2015.129>
- McCormick, B. J., & Chirila, R. M. (2021). Carnitine palmitoyltransferase-II deficiency: Case presentation and review of the literature. *Romanian Journal of Internal Medicine*, 59(4), 420–424. <https://doi.org/10.2478/rjim-2021-0021>
- McNally, B. D., Ashley, D. F., Hänschke, L., Daou, H. N., Watt, N. T., Murfitt, S. A., MacCannell, A. D. V., Whitehead, A., Bowen, T. S., Sanders, F. W. B., Vacca, M., Witte, K. K., Davies, G. R., Bauer, R., Griffin, J. L., & Roberts, L. D. (2022). Long-chain ceramides are cell non-autonomous signals linking lipotoxicity to endoplasmic reticulum stress in skeletal muscle. *Nature Communications*, 13(1), 1748. <https://doi.org/10.1038/s41467-022-29363-9>
- Merritt, J. L. 2nd, Norris, M., & Kanungo, S. (2018). Fatty acid oxidation disorders. *Annals of Translational Medicine*, 6(24), 473. <https://doi.org/10.21037/atm.2018.10.57>
- Mollazadeh, H., Tavana, E., Fanni, G., Bo, S., Banach, M., Pirro, M., von Haehling, S., Jamialahmadi, T., & Sahebkar, A. (2021). Effects of statins on mitochondrial pathways. *Journal of Cachexia, Sarcopenia and Muscle*, 12(2), 237–251. <https://doi.org/10.1002/jcsm.12654>
- Nagashima, S., Yagyu, H., Ohashi, K., Tazoe, F., Takahashi, M., Ohshiro, T., Bayasgalan, T., Okada, K., Sekiya, M., Osuga, J. I., & Ishibashi, S. (2012). Liver-specific deletion of 3-hydroxy-3-methylglutaryl coenzyme A reductase causes hepatic steatosis and death. *Arteriosclerosis, Thrombosis, and Vascular Biology*, 32(8), 1824–1831. <https://doi.org/10.1161/ATVBAHA.111.240754>
- Newman, C. B., Preiss, D., Tobert, J. A., Jacobson, T. A., Page, R. L. 2nd, Goldstein, L. B., Chin, C., Tannock, L. R., Miller, M., Raghuvver, G., Duell, P. B., Brinton, E. A., Pollak, A., Braun, L. T., Welty, F. K., & The American Heart Association Clinical Lipidology, Lipoprotein, Metabolism and Thrombosis Committee, a Joint Committee of the Council on Atherosclerosis, Thrombosis and Vascular Biology and Council on Lifestyle and Cardiometabolic Health; Council on Cardiovascular Disease in the Young; Council on Clinical Cardiology; and Stroke Council. (2019). Statin safety and associated adverse events: A scientific statement from the American Heart Association. *Arteriosclerosis, Thrombosis, and Vascular Biology*, 39(2), e38–e81. <https://doi.org/10.1161/ATV.0000000000000073>
- North, K. N., Hoppel, C. L., De Girolami, U., Kozakewich, H. P., & Korson, M. S. (1995). Lethal neonatal deficiency of carnitine palmitoyl-transferase II associated with dysgenesis of the brain and kidneys. *The Journal of Pediatrics*, 127(3), 414–420. [https://doi.org/10.1016/s0022-3476\(95\)70073-0](https://doi.org/10.1016/s0022-3476(95)70073-0)
- Okumoto, K., Tamura, S., Honsho, M., & Fujiki, Y. (2020). Peroxisome: Metabolic functions and biogenesis. *Advances in Experimental Medicine and Biology*, 1299, 3–17. [https://doi.org/10.1007/978-3-030-60204-8\\_1](https://doi.org/10.1007/978-3-030-60204-8_1)
- Okun, J. G., Kölker, S., Schulze, A., Kohlmüller, D., Olgemöller, K., Lindner, M., Hoffmann, G. F., Wanders, R. J. A., & Mayatepek, E. (2002). A method for quantitative acylcarnitine profiling in human skin fibroblasts using unlabelled palmitic acid: Diagnosis of fatty acid oxidation disorders and differentiation between biochemical phenotypes of MCAD deficiency. *Biochimica et Biophysica Acta*, 1584(2–3), 91–98. [https://doi.org/10.1016/s1388-1981\(02\)00296-2](https://doi.org/10.1016/s1388-1981(02)00296-2)
- Osaki, Y., Nakagawa, Y., Miyahara, S., Iwasaki, H., Ishii, A., Matsuzaka, T., Kobayashi, K., Yatoh, S., Takahashi, A., Yahagi, N., Suzuki, H., Sone, H., Ohashi, K., Ishibashi, S., Yamada, N., & Shimano, H. (2015). Skeletal muscle-specific HMG-CoA reductase knockout mice exhibit rhabdomyolysis: A model for statin-induced myopathy. *Biochemical and Biophysical Research Communications*, 466(3), 536–540. <https://doi.org/10.1016/j.bbrc.2015.09.065>
- Pang, Z., Chong, J., Zhou, G., de Lima Morais, D. A., Chang, L., Barrette, M., Gauthier, C., Jacques, P. É., Li, S., & Xia, J. (2021). MetaboAnalyst 5.0: Narrowing the gap between raw spectra and functional insights. *Nucleic Acids Research*, 49(W1), W388–W396. <https://doi.org/10.1093/nar/gkab382>
- Parker, B. A., Augeri, A. L., Capizzi, J. A., Ballard, K. D., Troyanos, C., Baggish, A. L., D'Heemecourt, P. A., & Thompson, P. D. (2012). Effect of statins on creatine kinase levels before and after a marathon run. *The American Journal of Cardiology*, 109(2), 282–287. <https://doi.org/10.1016/j.amjcard.2011.08.045>
- Penson, P. E., Bruckert, E., Marais, D., Reiner, Z., Pirro, M., Sahebkar, A., International Lipid Expert Panel (ILEP), Bajraktari, G., Mirrahimov, E., Rizzo, M., Mikhailidis, D. P., Sachinidis, A., Gaita, D., Latkovskis, G., Mazidi, M., Toth, P. P., Pella, D., Alnouri, F., Postadzhiyan, A., ... Banach, M. (2022). Step-by-step diagnosis and management of the nocebo/drucebo effect in statin-associated muscle symptoms patients: A position paper from the International Lipid Expert Panel (ILEP). *Journal of Cachexia, Sarcopenia and Muscle*, 13(3), 1596–1622. <https://doi.org/10.1002/jcsm.12960>
- Percie du Sert, N., Hurst, V., Ahluwalia, A., Alam, S., Avey, M. T., Baker, M., Browne, W. J., Clark, A., Cuthill, I. C., Dirnagl, U., Emerson, M., Garner, P., Holgate, S. T., Howells, D. W., Karp, N. A., Lazic, S. E., Lidster, K., MacCallum, C. J., Macleod, M., ... Würbel, H. (2020). The ARRIVE guidelines 2.0: Updated guidelines for reporting animal research. *PLoS Biology*, 18(7), e3000410. <https://doi.org/10.1371/journal.pbio.3000410>
- Pessayre, D., Fromenty, B., Berson, A., Robin, M. A., Letteron, P., Moreau, R., & Mansouri, A. (2012). Central role of mitochondria in drug-induced liver injury. *Drug Metabolism Reviews*, 44(1), 34–87. <https://doi.org/10.3109/03602532.2011.604086>
- Piccinin, E., Villani, G., & Moschetta, A. (2019). Metabolic aspects in NAFLD, NASH and hepatocellular carcinoma: The role of PGC1 coactivators. *Nature Reviews. Gastroenterology & Hepatology*, 16(3), 160–174. <https://doi.org/10.1038/s41575-018-0089-3>
- Primassin, S., Ter Veld, F., Mayatepek, E., & Spiekeroetter, U. (2008). Carnitine supplementation induces acylcarnitine production in tissues of very long-chain acyl-CoA dehydrogenase-deficient mice, without replenishing low free carnitine. *Pediatric Research*, 63(6), 632–637. <https://doi.org/10.1203/PDR.0b013e31816ff6f0>
- Puigserver, P., Rhee, J., Donovan, J., Walkey, C. J., Yoon, J. C., Oriente, F., Kitamura, Y., Altomonte, J., Dong, H., Accili, D., & Spiegelman, B. M. (2003). Insulin-regulated hepatic gluconeogenesis through FOXO1–PGC-1 $\alpha$  interaction. *Nature*, 423(6939), 550–555. <https://doi.org/10.1038/nature01667>
- Russell, D. W. (2003). The enzymes, regulation, and genetics of bile acid synthesis. *Annual Review of Biochemistry*, 72, 137–174. <https://doi.org/10.1146/annurev.biochem.72.121801.161712>
- Schirris, T. J., Renkema, G. H., Ritschel, T., Voermans, N. C., Bilos, A., van Engelen, B. G., Brandt, U., Koopman, W. J. H., Beyrath, J. D.,

- Rodenburg, R. J., Willems, P. H. G. M., Smeitink, J. A. M., & Russel, F. G. M. (2015). Statin-induced myopathy is associated with mitochondrial complex III inhibition. *Cell Metabolism*, 22(3), 399–407. <https://doi.org/10.1016/j.cmet.2015.08.002>
- Schuster, S., Cabrera, D., Arrese, M., & Feldstein, A. E. (2018). Triggering and resolution of inflammation in NASH. *Nature Reviews. Gastroenterology & Hepatology*, 15(6), 349–364. <https://doi.org/10.1038/s41575-018-0009-6>
- Shriver, L. P., & Manchester, M. (2011). Inhibition of fatty acid metabolism ameliorates disease activity in an animal model of multiple sclerosis. *Scientific Reports*, 1, 79. <https://doi.org/10.1038/srep00079>
- Spiekerkoetter, U., Lindner, M., Santer, R., Grotzke, M., Baumgartner, M. R., Boehles, H., das, A., Haase, C., Hennermann, J. B., Karall, D., de Klerk, H., Knerr, I., Koch, H. G., Plecko, B., Röschinger, W., Schwab, K. O., Scheible, D., Wijburg, F. A., Zschocke, J., ... Wendel, U. (2009). Management and outcome in 75 individuals with long-chain fatty acid oxidation defects: Results from a workshop. *Journal of Inherited Metabolic Disease*, 32(4), 488–497. <https://doi.org/10.1007/s10545-009-1125-9>
- Su, Q., Baker, C., Christian, P., Naples, M., Tong, X., Zhang, K., Santha, M., & Adeli, K. (2014). Hepatic mitochondrial and ER stress induced by defective PPAR $\alpha$  signaling in the pathogenesis of hepatic steatosis. *American Journal of Physiology. Endocrinology and Metabolism*, 306(11), E1264–E1273. <https://doi.org/10.1152/ajpendo.00438.2013>
- Takei, S., Nagashima, S., Takei, A., Yamamuro, D., Wakabayashi, T., Murakami, A., Isoda, M., Yamazaki, H., Ebihara, C., Takahashi, M., Ebihara, K., Dezaki, K., Takayanagi, Y., Onaka, T., Fujiwara, K., Yashiro, T., & Ishibashi, S. (2020).  $\beta$ -Cell-specific deletion of HMG-CoA (3-hydroxy-3-methylglutaryl-coenzyme A) reductase causes overt diabetes due to reduction of  $\beta$ -cell mass and impaired insulin secretion. *Diabetes*, 69(11), 2352–2363. <https://doi.org/10.2337/db19-0996>
- Tominaga, H., Katoh, H., Odagiri, K., Takeuchi, Y., Kawashima, H., Saotome, M., Urushida, T., Satoh, H., & Hayashi, H. (2008). Different effects of palmitoyl-L-carnitine and palmitoyl-CoA on mitochondrial function in rat ventricular myocytes. *American Journal of Physiology. Heart and Circulatory Physiology*, 295(1), H105–H112. <https://doi.org/10.1152/ajpheart.01307.2007>
- Tonelli, C., Chio, I. I. C., & Tuveson, D. A. (2018). Transcriptional regulation by Nrf2. *Antioxidants & Redox Signaling*, 29(17), 1727–1745. <https://doi.org/10.1089/ars.2017.7342>
- Vega, R. B., Huss, J. M., & Kelly, D. P. (2000). The coactivator PGC-1 cooperates with peroxisome proliferator-activated receptor  $\alpha$  in transcriptional control of nuclear genes encoding mitochondrial fatty acid oxidation enzymes. *Molecular and Cellular Biology*, 20(5), 1868–1876. <https://doi.org/10.1128/MCB.20.5.1868-1876.2000>
- Ventura, F. V., Costa, C. G., Struys, E. A., Ruiten, J., Allers, P., Ijlst, L., Tavares de Almeida, I., Duran, M., Jakobs, C., & Wanders, R. J. A. (1999). Quantitative acylcarnitine profiling in fibroblasts using [ $^{13}\text{C}$ ] palmitic acid: An improved tool for the diagnosis of fatty acid oxidation defects. *Clinica Chimica Acta*, 281(1–2), 1–17. [https://doi.org/10.1016/s0009-8981\(98\)00188-0](https://doi.org/10.1016/s0009-8981(98)00188-0)
- Virani, S. S., Akeroyd, J. M., Nambi, V., Heidenreich, P. A., Morris, P. B., Nasir, K., Michos, E. D., Bittner, V. A., Petersen, L. A., & Ballantyne, C. M. (2017). Estimation of eligibility for proprotein convertase subtilisin/kexin type 9 inhibitors and associated costs based on the FOURIER trial (Further Cardiovascular Outcomes Research With PCSK9 Inhibition in Subjects With Elevated Risk): Insights from the Department of Veterans Affairs. *Circulation*, 135(25), 2572–2574. <https://doi.org/10.1161/CIRCULATIONAHA.117.028503>
- Vladutiu, G. D., Simmons, Z., Isackson, P. J., Tarnopolsky, M., Peltier, W. L., Barboi, A. C., Sripathi, N., Wortmann, R. L., & Phillips, P. S. (2006). Genetic risk factors associated with lipid-lowering drug-induced myopathies. *Muscle & Nerve*, 34(2), 153–162. <https://doi.org/10.1002/mus.20567>
- Wanders, R. J. A., Visser, G., Ferdinandusse, S., Vaz, F. M., & Houtkooper, R. H. (2020). Mitochondrial fatty acid oxidation disorders: Laboratory diagnosis, pathogenesis, and the complicated route to treatment. *Journal of Lipid and Atherosclerosis*, 9(3), 313–333. <https://doi.org/10.12997/jla.2020.9.3.313>
- Wu, T., Hu, E., Xu, S., Chen, M., Guo, P., Dai, Z., Feng, T., Zhou, L., Tang, W., Zhan, L., Fu, X., Liu, S., Bo, X., & Yu, G. (2021). clusterProfiler 4.0: A universal enrichment tool for interpreting omics data. *Innovation (Camb)*, 2(3), 100141. <https://doi.org/10.1016/j.xinn.2021.100141>
- Wu, Z., Puigserver, P., Andersson, U., Zhang, C., Adelmant, G., Mootha, V., Troy, A., Cinti, S., Lowell, B., Scarpulla, R. C., & Spiegelman, B. M. (1999). Mechanisms controlling mitochondrial biogenesis and respiration through the thermogenic coactivator PGC-1. *Cell*, 98(1), 115–124. [https://doi.org/10.1016/S0092-8674\(00\)80611-X](https://doi.org/10.1016/S0092-8674(00)80611-X)
- Yeh, Y. S., Jheng, H. F., Iwase, M., Kim, M., Mohri, S., Kwon, J., Kawarasaki, S., Li, Y., Takahashi, H., Ara, T., Nomura, W., Kawada, T., & Goto, T. (2018). The mevalonate pathway is indispensable for adipocyte survival. *iScience*, 9, 175–191. <https://doi.org/10.1016/j.isci.2018.10.019>
- Zhang, P., Konja, D., Zhang, Y., & Wang, Y. (2021). Communications between mitochondria and endoplasmic reticulum in the regulation of metabolic homeostasis. *Cells*, 10, 2195. <https://doi.org/10.3390/cells10092195>

## SUPPORTING INFORMATION

Additional supporting information can be found online in the Supporting Information section at the end of this article.

**How to cite this article:** Liepinsh, E., Zvejniece, L., Clemensson, L., Ozola, M., Vavers, E., Cirule, H., Korzh, S., Skuja, S., Groma, V., Briviba, M., Grinberga, S., Liu, W., Olszewski, P., Gentreau, M., Fredriksson, R., Dambrova, M., & Schiöth, H. B. (2024). Hydroxymethylglutaryl-CoA reductase activity is essential for mitochondrial  $\beta$ -oxidation of fatty acids to prevent lethal accumulation of long-chain acylcarnitines in the mouse liver. *British Journal of Pharmacology*, 181(16), 2750–2773. <https://doi.org/10.1111/bph.16363>